Published in International Journal of Pressure Vessels and Piping (doi:10.1016/j.ijpvp.2010.07.010)

A review of the effect of prior inelastic deformation on high temperature mechanical response of engineering alloys

D.F. Li[†], N.P. O'Dowd[†,§], C.M. Davies[‡], K.M. Nikbin[‡]
[†]Department of Mechanical & Aeronautical Engineering
Materials & Surface Science Institute
University of Limerick, Limerick, Ireland
[‡]Department of Mechanical Engineering
Imperial College London, United Kindom
[§]Corresponding author. Tel.: +353 61202545; fax: +353 61233766
E-mail address: noel.odowd@ul.ie

June 28, 2010

Abstract

In this review article, we examine the influence of prior deformation (prestrain) on the subsequent high temperature mechanical behaviour of engineering alloys. We review the observed effects at a macroscopic level in terms of creep deformation, creep rupture times and crack growth rates from a number of sources and a range of materials. Microstructural explanations for the observed macroscopic effects are also reviewed and constitutive models which incorporate the effect of prior deformation are examined. The emphasis in the paper is on engineering steels though reference is also made to non ferrous alloys.
Keywords: Steel; Experimental stress analysis; Fracture mechanics; Creep deformation; Power plants

1 Introduction

Prior deformation, e.g., hot or cold working, has been recognised as an important route to strengthen metallic materials by creating dislocation barriers to inhibit subsequent dislocation movement during plastic deformation at room temperature (see, e.g., [1]). In many practical cases metallic materials operate at an elevated temperature. Under these conditions, the deformation behaviour typically exhibits history, rate and environmental dependencies, governed by microstructural evolution, due to dislocation movement and diffusion processes. Therefore, examining the influence of prior deformation on subsequent high temperature

creep and creep fracture behaviour is a topic of significant theoretical and practical interest in e.g., conventional/nuclear power plant, where components are often in a prestrained condition; aerospace engines, where turbine components are often exposed to cyclic thermal and mechanical loading; and combustors, where components experience creep at high temperatures and plastic deformation at low temperatures. To optimize the component performance or to create optimal creep-resistant materials, a theoretical understanding is needed to quantify the creep response changes caused by prior deformation, and to identify the underlying mechanisms.

Since the 1960s, efforts have been made to consider the effect of prior deformation (prestrain) on the subsequent high temperature creep of engineering metallic materials. Yet, because high temperature creep, as a complex multi-physics-coupled phenomenon, is sensitive to many factors, e.g., material composition and microstructure, operating conditions (temperature and stress level) and sample geometry, several seemingly conflicting outcomes of prior deformation have been reported. For example, Wilshire and Willis [2] found that prestrain at room temperature for 316H/L stainless steel can increase creep resistance; Zhang and Knowles [3] showed a contrary effect for nickel base C263 superalloy where prestrain reduces creep resistance. Thus, the purpose of this work is to review published studies in the field of prior-deformation effects on subsequent high temperature creep for metallic materials to gain an overall understanding of this topic. The emphasis in the paper is on engineering steels though reference is also made to non ferrous alloys.

The paper is laid out as follows: Section 2 reviews the measured macroscopic effects of prior deformation on creep response at high temperature by comparing the creep response of pre-deformed samples and as-received samples. In Section 3, the evidence of microstructural changes due to prior deformation is summarised to investigate a physical interpretation of the effects. Section 4 examines the development of numerical investigations in this topic. In Section 5, a summary is provided.

2 Macroscopic effects of prior inelastic deformation

There have been a number of experimental investigations to examine the role that prior deformation plays in subsequent mechanical response at high temperature. This section reviews these investigations, focusing in particular on the effects reported in macroscopic creep tests, the materials examined in these studies, the type of prior deformation (e.g. pre-tension or pre-compression), the geometry of specimens and the operating temperature. In order to understand clearly the mechanisms behind these observed effects, we first differentiate the literature into two groups according to the observed influence on creep deformation, namely 'creep resistance effects' and 'creep enhancement effects'. The former term refers to a measured reduction in creep strain rates following prior deformation and the latter a measured increase in creep strain rates. In addition to the effects on creep deformation, prior deformation can also introduce important effects on creep fracture behaviour, typically represented by changes in creep life, creep ductility and creep crack growth which are also discussed in this section.

2.1 Creep resistance effects

The phenomenon that creep deformation can be impeded by prestrain has been widely reported for engineering steels (see, e.g., [2, 4–6]). By employing thin-wall tubes of 316H stainless steel as creep test specimens (outside diameter, wall thickness and gauge length are 21 mm, 1 mm and 70 mm, respectively), Ohashi et al. [4] examined the effect of pre-tension on subsequent creep at elevated temperature (650°C). The specimens were soaked uniformly for 20 hours at 650°C, and uniaxial plastic pretensions were then applied to the specimens (1%, 2% and 3% prestrains corresponding to applied stresses of 174 MPa, 196 MPa and 218 MPa, respectively). Creep tests in tension and torsion were subsequently conducted at a constant stress of 140 MPa at the same temperature. Figure 1 shows the marked creep resistance effect introduced by prestrain in these tests. It can be seen that at $t = 100$ hours the creep strain for the specimen subjected to a prestrain of 1% is reduced by almost 50% compared to the as-received specimen. In Fig. 2, it is shown that with increasing pretension the subsequent creep strain under torsional loading is also reduced significantly. The stress indicated in Fig. 2, σ_{eq}, is the von Mises equivalent stress,

$$\sigma_{eq} = \frac{1}{\sqrt{2}}\sqrt{(\sigma_1 - \sigma_2)^2 + (\sigma_2 - \sigma_3)^2 + (\sigma_3 - \sigma_1)^2}, \tag{1}$$

where σ_1, σ_2 and σ_3 are principal stresses, and the strain $\bar{\varepsilon}$, is the von Mises equivalent strain (also called effective strain),

$$\bar{\varepsilon} = \frac{\sqrt{2}}{3}\sqrt{(\varepsilon_1 - \varepsilon_2)^2 + (\varepsilon_2 - \varepsilon_3)^2 + (\varepsilon_3 - \varepsilon_1)^2} \tag{2}$$

where ε_1, ε_2 and ε_3 are principal strains.

Similar trends have been reported in [5] using uniaxial specimens of AISI 304 stainless steel with 20 mm gauge length and 3 mm diameter. In these tests the effects of prestrain at higher temperature than the subsequent creep test temperature were examined. Specimens were first prestrained at 650°C, 700°C and 750°C, respectively under a constant stress level leading to elongations of up to 4.5%. Specimens were then cooled to the creep test temperature of 600°C and a creep test was conducted at the same stress level as used for pre-tension. Figure 3 shows that prestraining at 700°C leads to a reduced creep strain at the lower temperature. In addition, Fig. 4 shows the effect of prestrain at different temperatures on creep rate. It can be seen that the higher the prestraining temperature, the lower the creep resistance effect.

The investigations above focus on the effects of high temperature prestrain. Resistance effects are also identified for prestrain at room temperature. Usami and Mori [6] investigated the creep deformation of austenitic steels at low temperatures (140°C). The effects of prestrain (pretension) at room temperature were studied using small uniaxial creep specimens with a square test section ($4 \times 4 \times 8$ mm). The results in Fig. 5 show that room temperature prestrain can also lead to an increase of creep resistance. Note that at these temperatures and stresses the material demonstrates logarithmic creep (creep strain increasing linearly with $\log(t)$).

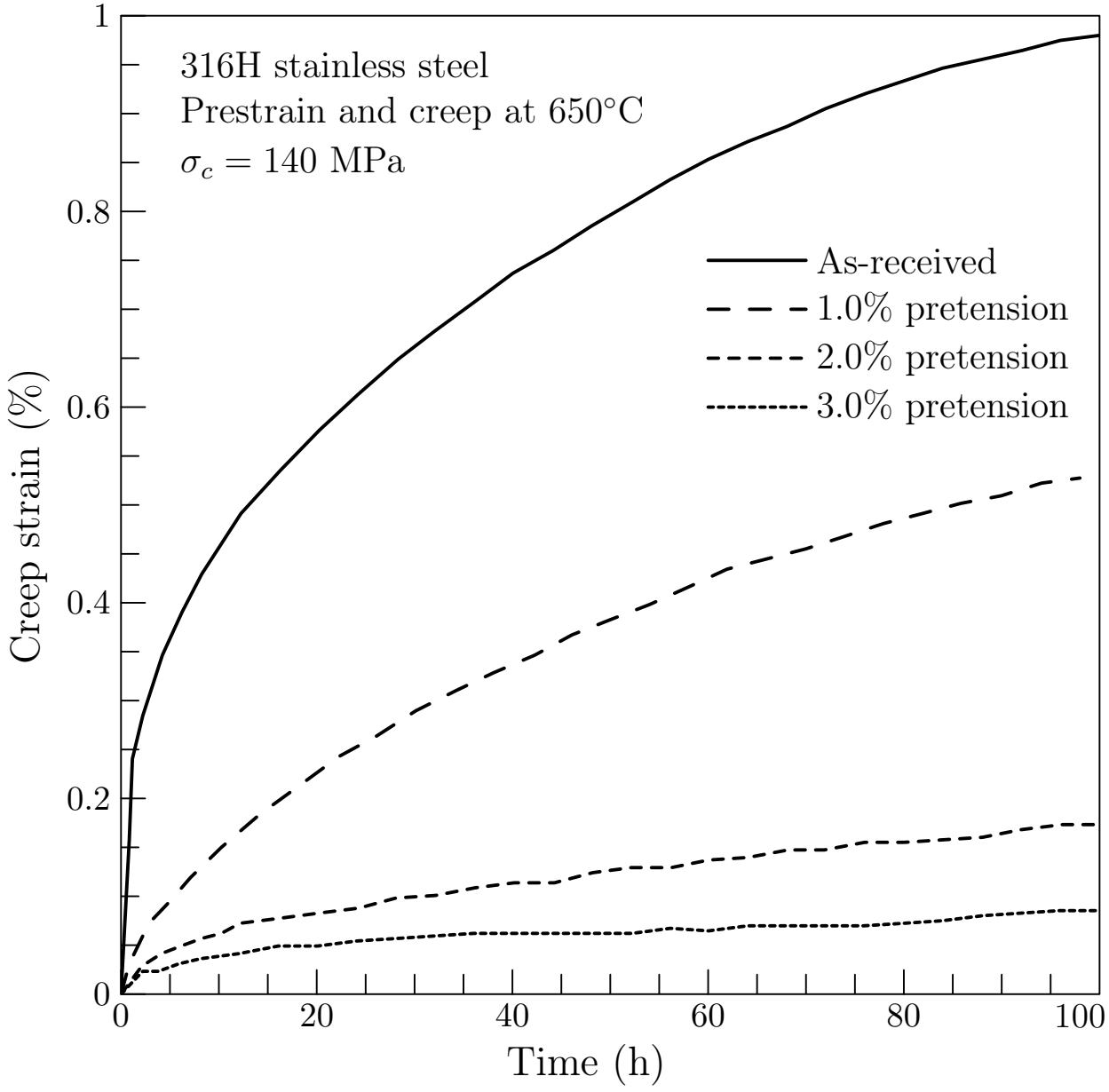

Figure 1: Effect of prestrain on creep of 316H stainless steel under uniaxial tension (Adapted from [4]).

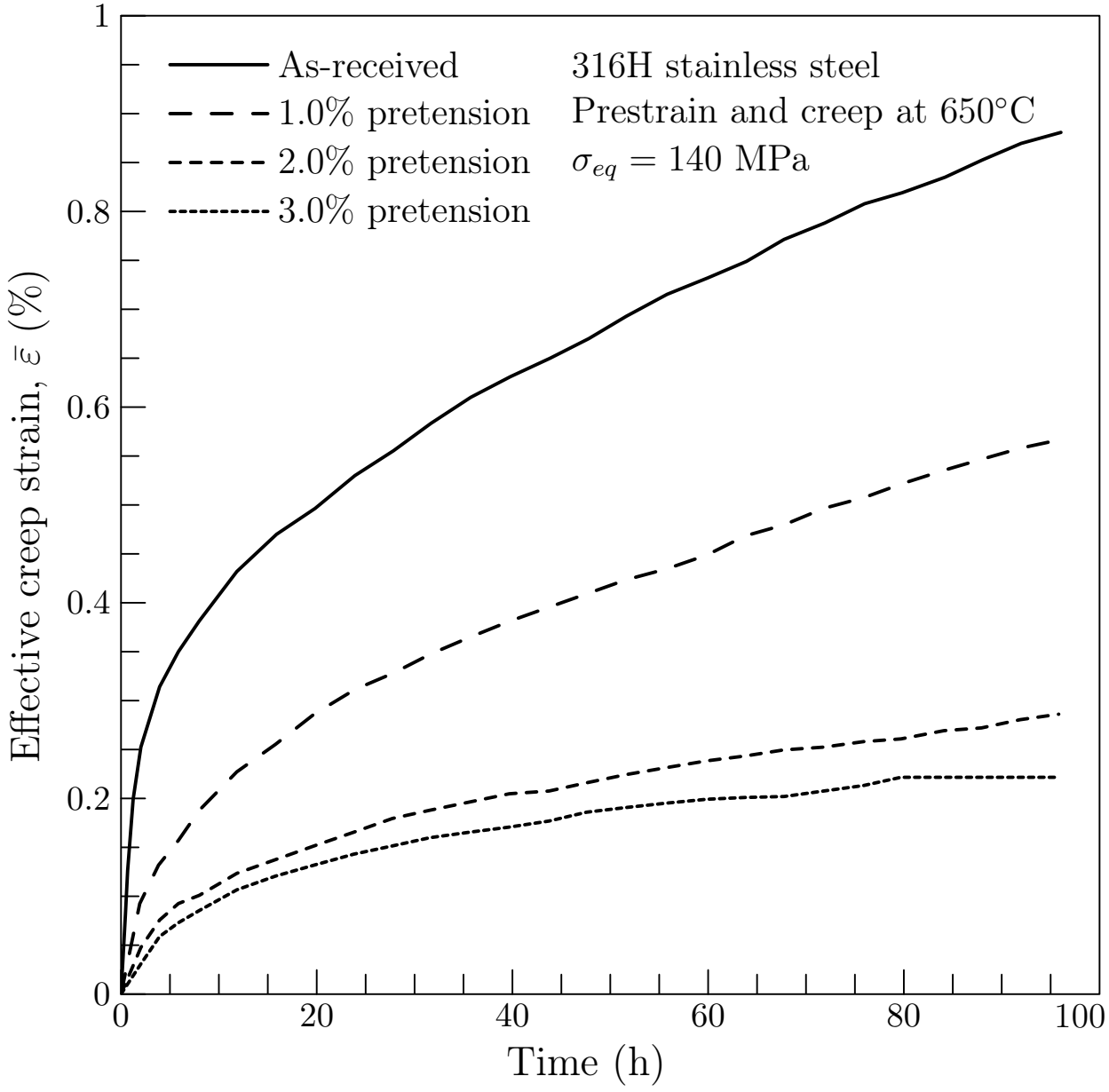

Figure 2: Effect of prestension on creep of 316H stainless steel under torsional loading (Adapted from [4]).

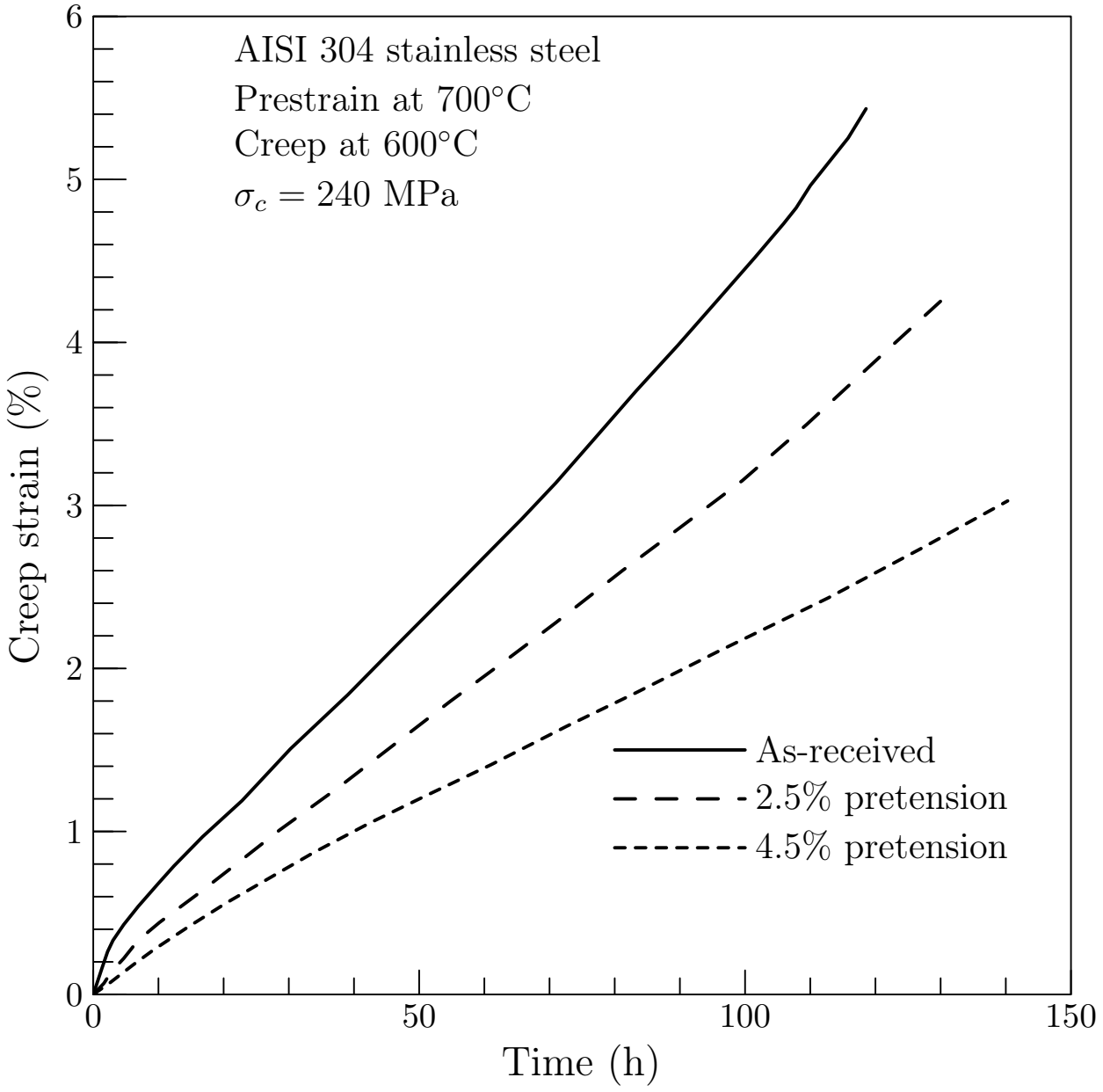

Figure 3: Prestraining results in [5] for 304 stainless steel (Adapted from [5]).

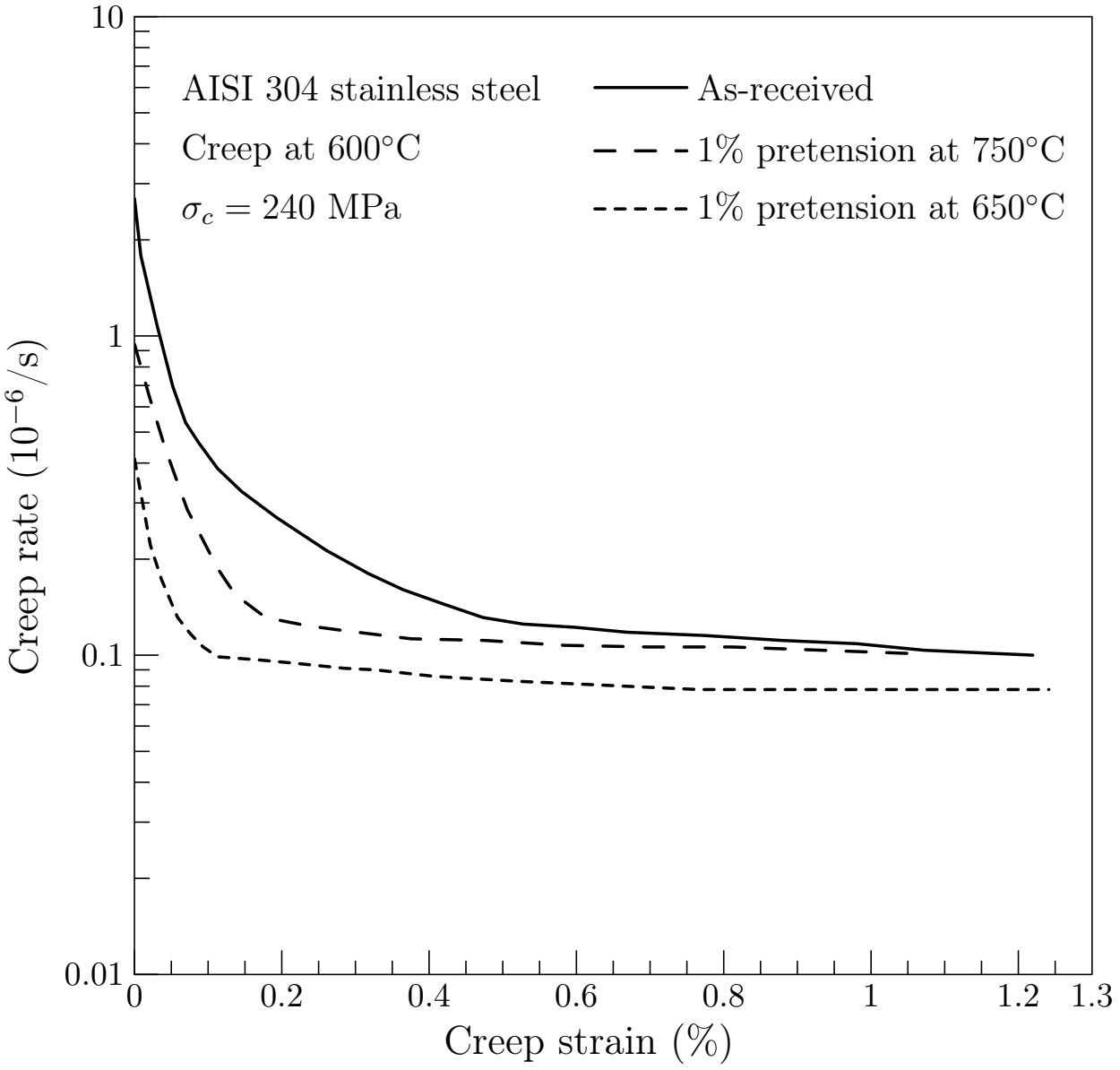

Figure 4: Effect of prestrain at various temperatures for 304 stainless steel (Adapted from [5]).

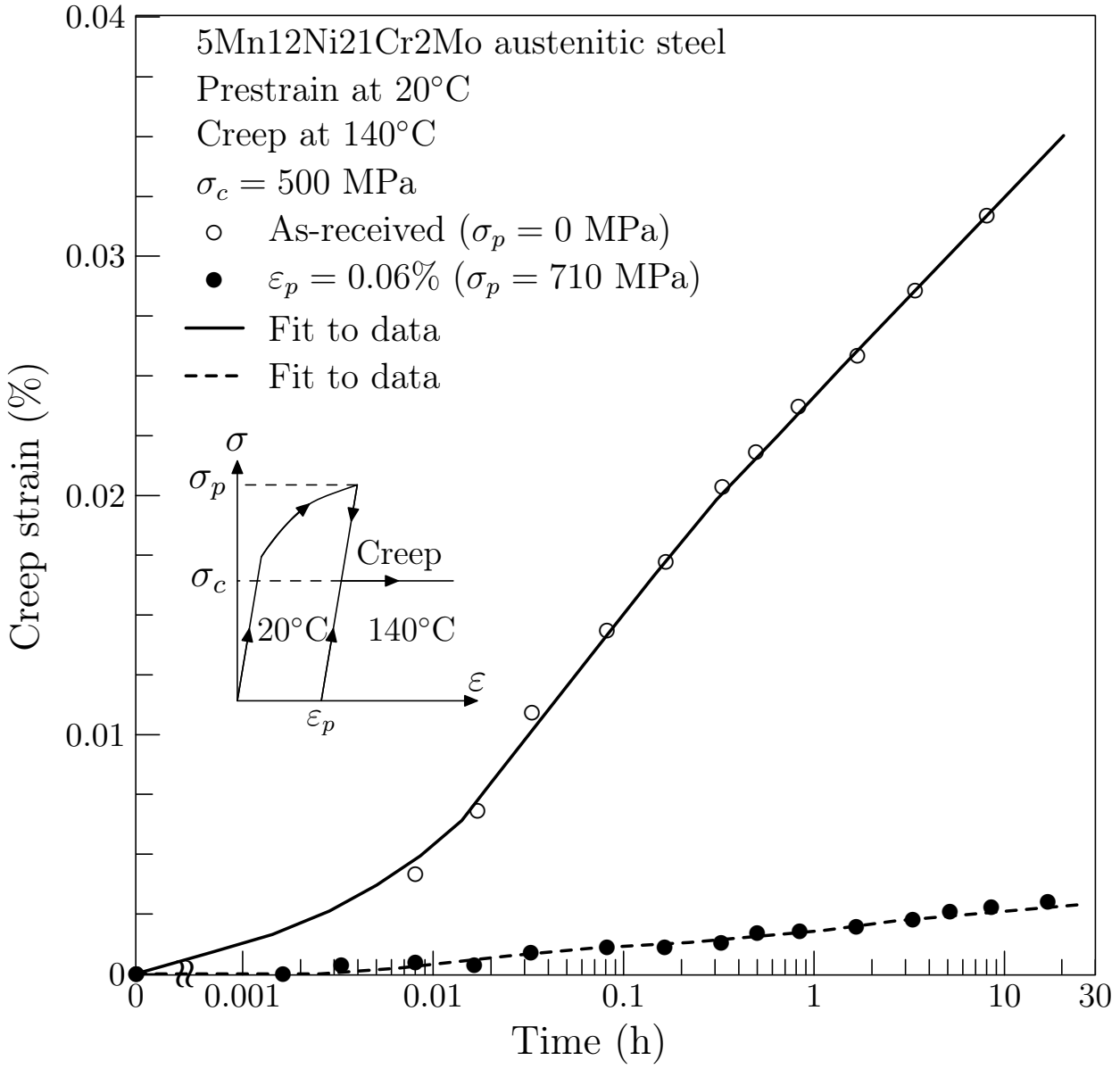

Figure 5: Room temperature prestraining effect on creep response of 5Mn12Ni21Cr2Mo austenitic steel at 500 MPa and 140°C (Adapted from [6]).

Wilshire and Willis [2] studied the effects of pretension at room and elevated temperature (575°C) for 316L and 316H stainless steels, using cylindrical test pieces with 25.4 mm gauge length and 3.8 mm diameter. According to the solution treatments employed, the as-received materials were divided into three groups, namely partially solution-treated (PST) 316H stainless steel; fully solution-treated (FST) 316H stainless steel; and FST 316L stainless steel. The creep response of the three material groups to different amounts of prestrain at room temperature are shown in Figs. 6, 7 and 8. It may be seen that the creep strain drops significantly following room temperature prestraining. Furthermore, it may be seen that the magnitude of the effect is sensitive to material with a much weaker effect observed for the PST 316H material under similar conditions. The effects of high-temperature creep prestrain were also examined in [2]. It was found that there was a drop in creep rate in the primary stage of creep which results in a reduction in creep strain similar to the results in [5].

Resistance effects on creep have been also reported for polycrystalline and single crystalline nonferrous alloys. Davies et al. [7] reported that room temperature prestrain can improve creep resistance at 500°C for polycrystalline nickel alloy at low stress level; Marlin et al. [8] reported that the creep rate at 760°C may decrease with increasing creep prestrain at the same temperature for an oxide dispersion strengthened Nickel-base alloy; Wang et al. [9] found that for TiAl alloys at high temperature (760°C or 815°C) primary creep can be significantly reduced by pretension at a higher stress level; Cairney et al. [10] found that both room and high temperature creep prestrain can decrease the subsequent creep strain at 520°C for single-crystal Ni_3Al and high temperature prestrain has a greater effect than room temperature prestrain. The latter result is contrary to the results in [5] for ferrous materials (Fig. 3).

2.2 Creep enhancement effects

A creep enhancing effect (prestrain reducing creep resistance) has also been reported for engineering steels, nonferrous alloys and pure metals.

Davies et al. [11] examined the effect of compressive prestrain on unaxial creep deformation of 316H stainless steel at 550°C. In this study, blocks of material were compressed uniformly at room temperature to produce plastic strains of 4% and 8%, respectively. Uniaxial creep specimens with 25 mm gauge length and 8 mm diameter [12] were then manufactured from the compressed blocks. Figure 9 shows the creep curves of as-received and prestrained (precompression) materials. It is seen that the compressive prestrain leads to significant enhancements of creep strain.

Tai and Endo [13] investigated the role that creep prestrain at 600°C plays in the subsequent creep response at the same temperature, using test specimens of 2.25Cr-1Mo steel (30 mm gage length; 6 mm diameter). Specimens were subjected to creep loading at 98 MPa up to a certain level of prestrain ($0.14\% \leq \varepsilon_p \leq 19.4\%$) and then reloaded under creep conditions at a different stress level.

To quantify the effect of prestrain, an enhancement parameter, Φ, was introduced

$$\Phi = \frac{\dot{\varepsilon}^p_{min}}{\dot{\varepsilon}_{min}}, \tag{3}$$

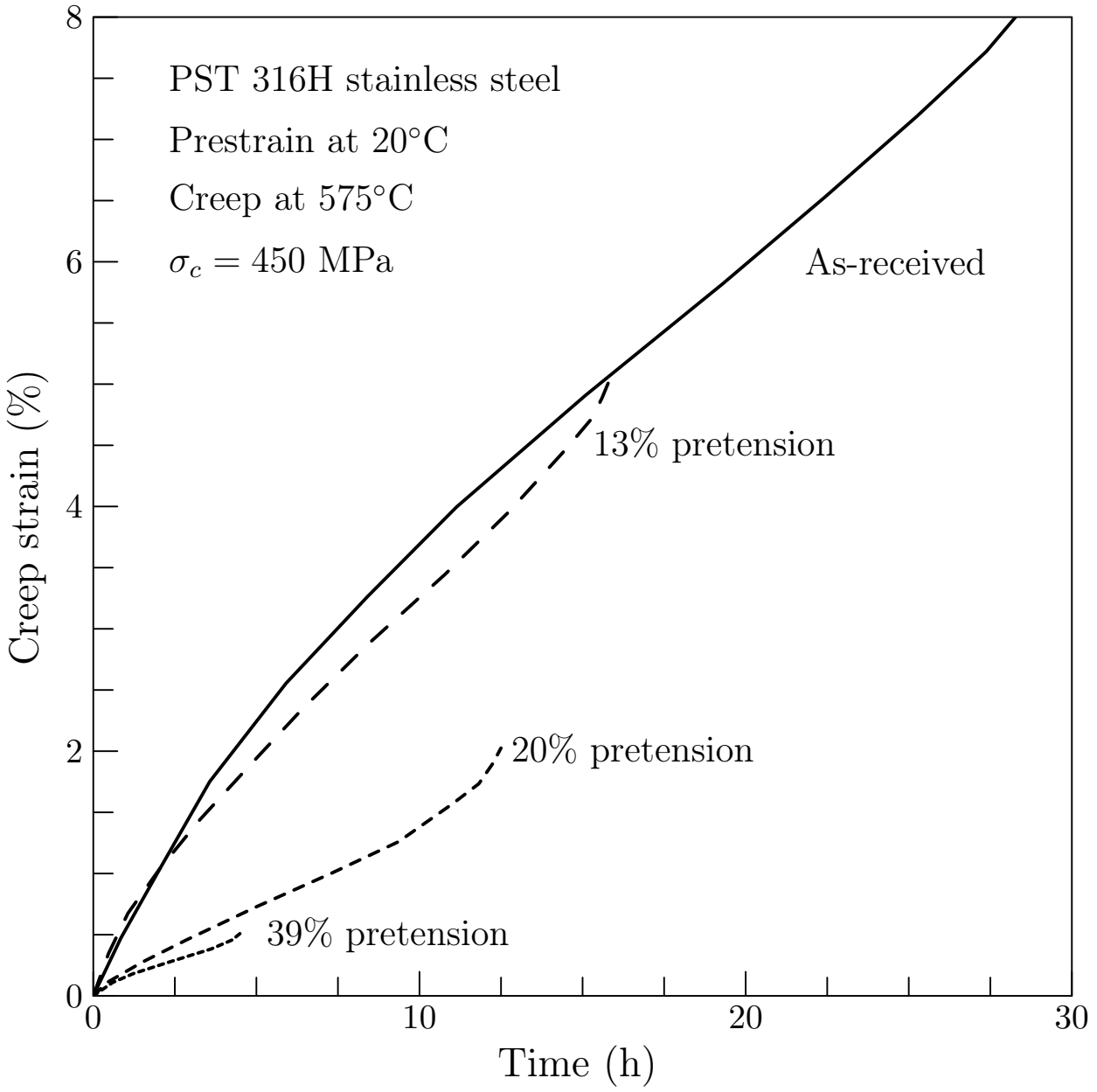

Figure 6: Creep responses at 450 MPa and 575°C of PST 316H stainless steel with different room temperature prestrains (Adapted from [2]).

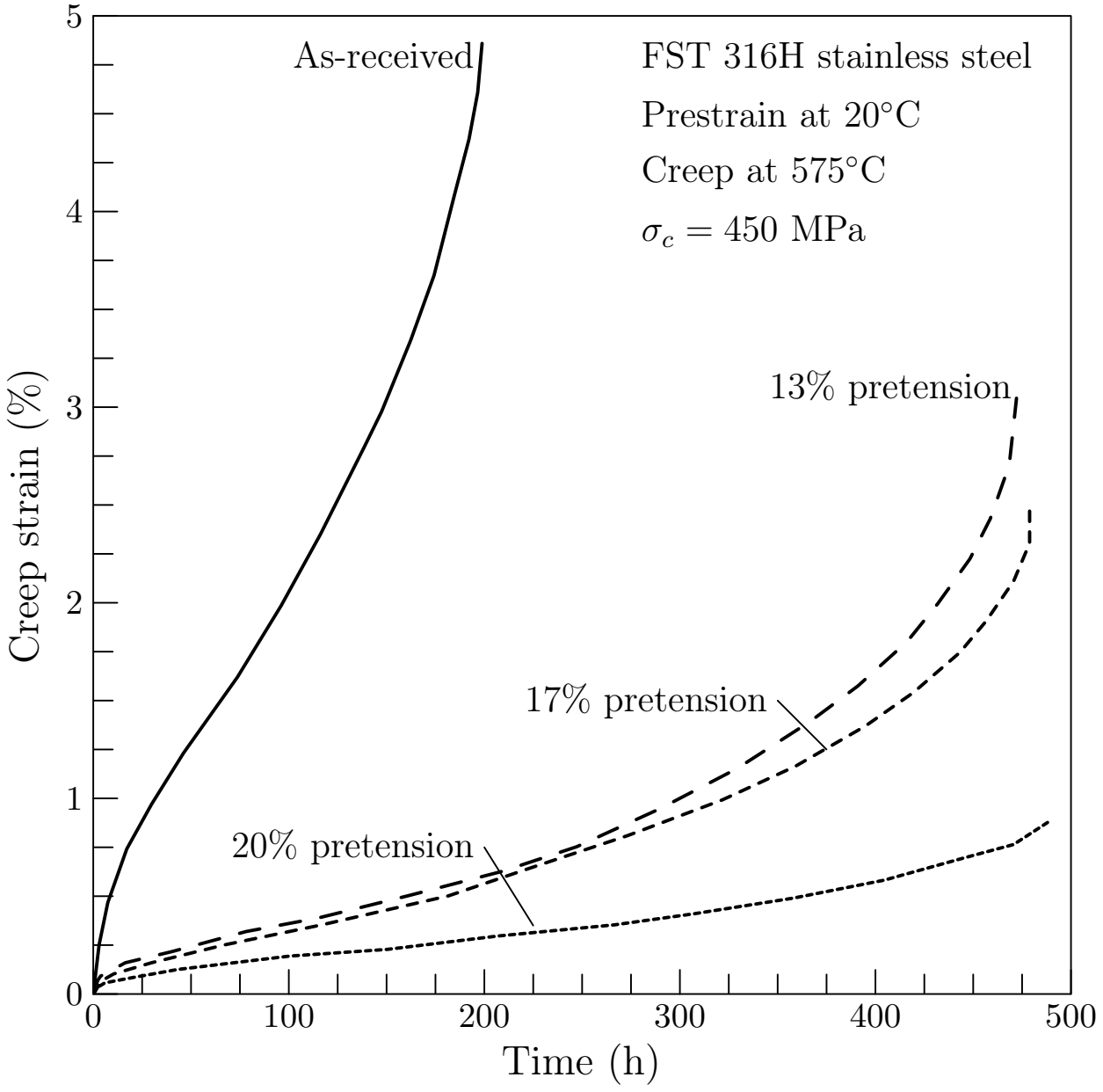

Figure 7: Creep responses at 450 MPa and 575°C of FST 316H stainless steel with different room temperature prestrains (Adapted from [2]).

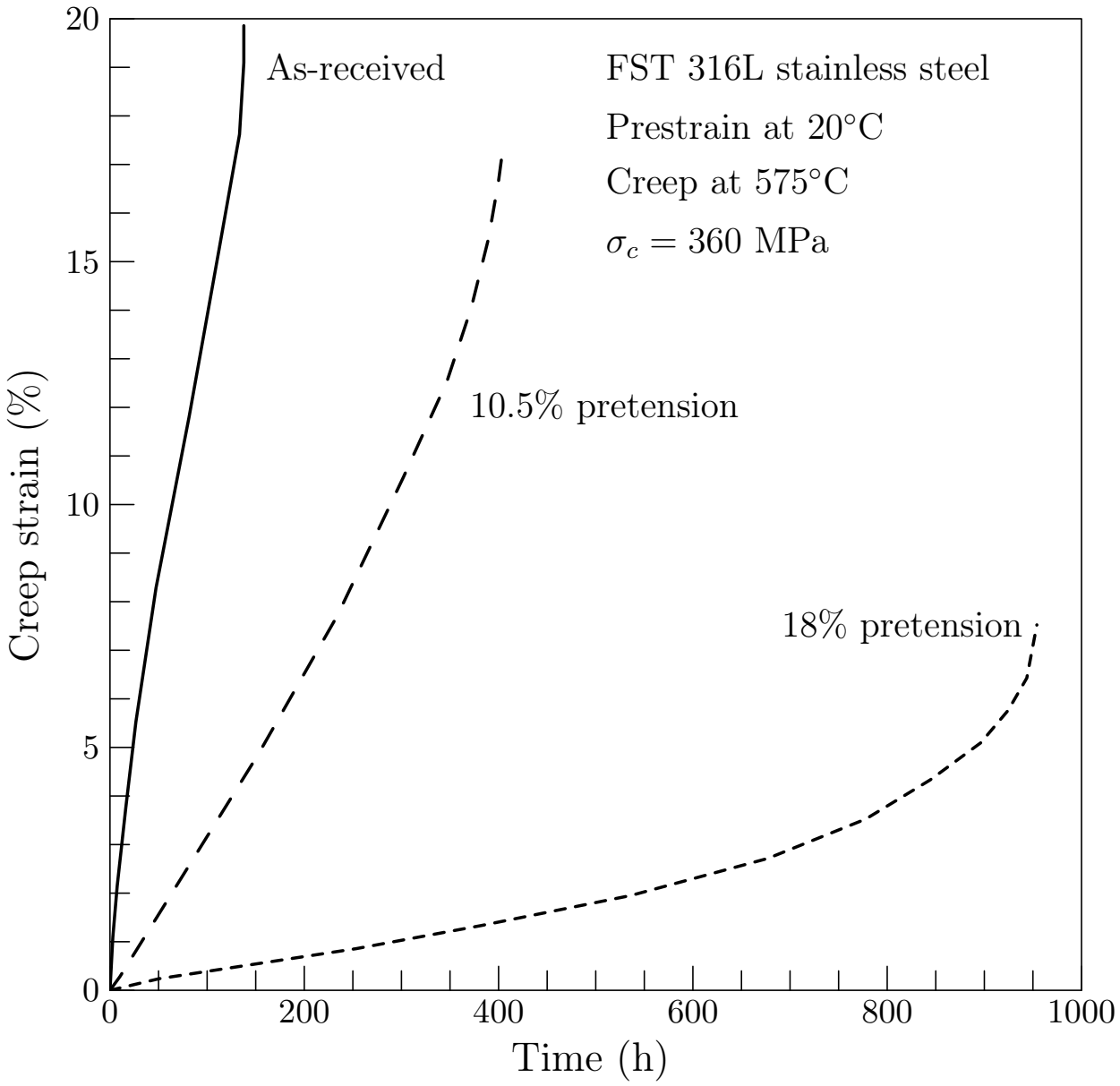

Figure 8: Creep responses at 360 MPa and 575°C of FST 316L stainless steel with different room temperature prestrains (Adapted from [2]).

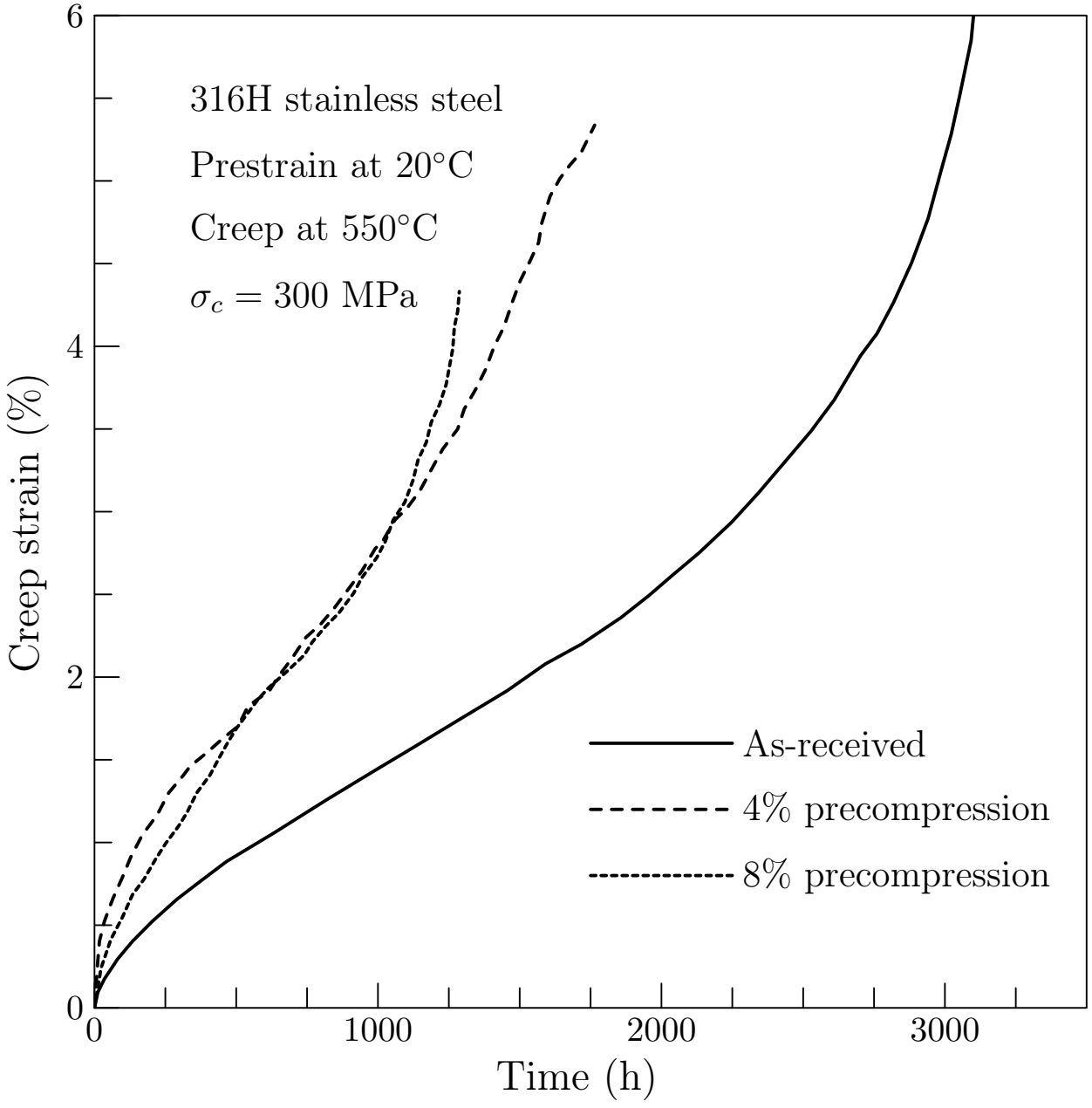

Figure 9: Creep curves at 550°C and 300 MPa for 316H stainless steel as-received and after prior deformation by 4% and 8% compression at room temperature (Adapted from [11]).

where $\dot{\varepsilon}^p_{min}$ and $\dot{\varepsilon}_{min}$ denote the minimum creep rates of prestrained and as-received specimens, respectively. $\Phi = 1$ implies no effect of prestrain, $\Phi > 1$ implies enhancement and vice versa. Figure 10 shows the variation of Φ as a function of prestrain at 600°C, which reveals that over a range of stress levels $\Phi > 1$ and Φ increases with increasing prestrain. Note that Figure 10 shows a data point where prestrain and subsequent creep are at the same applied stress ($\sigma_0 = \sigma_c = 98$ MPa, for a pre-strain of approx. 1%). In this case the enhancement parameter is approx. 2, which is somewhat surprising, implying that the minimum creep rate of an interrupted creep test may be twice that of a continuous creep test. The observed effect may be due to experimental scatter (note that the best fit line is close to unity for this data point), due to the additional damage introduced during the pre-strain cycle, or due to the aging effect during prestrain. However, note that in [13] the aging effect was concluded to be small (prestraining time does not exceed 60 hours). Note also for the largest prestrain level in Fig. 10 (19.4%) the enhancement factor can be as high as 8. This large creep enhancement may be due to the introduction of inelastic damage during the pre-strain cycle. As will be discussed in Section 2.3, for some of these data points the prestrain may be close to the creep ductility of the material

For nonferrous alloys, Dayson et al. [14] carried out a series of tests on Nimonic 80A using thin-walled tubular torsion specimens (16 mm gauge length; 0.8 mm wall thickness; 8.0 mm outer diameter) to examine the effect of prior torsion at room temperature on subsequent high temperature creep in torsion. Figure 11 shows that for this material pre-torsion leads to an increase in creep strain. In Fig. 11 the term "forward creep" indicates that the torque applied under creep conditions is in the same direction as that applied during room temperature pre-torsion, while the term "reverse creep" implies that the direction of torsion during creep is reversed. It may be noted that the creep enhancement is larger for reverse creep than for forward creep.

Loveday and Dyson [15] examined the effect of room temperature pretension on subsequent creep deformation of nickel base superalloy, IN597, at 800°C. After a prestrain of 9% there is a large increase in creep rate. Pandey et al. [16] found that pretension at room temperature led to creep enhancement for the creep response of Inconel alloy X-750 at 750°C.

Rong et al. [17] studied the effects of precompression at room temperature and 800°C on the subsequent primary compressive creep response of polycrystalline single-phase titanium aluminide. Figure 12 shows the creep curves of as-received and prestrained materials. It is found that precompression at room temperature or 800°C can increase the subsequent primary compressive creep at 800°C and both primary and secondary creep rate are increased for high temperature precompression. Zhang and Knowles [3] examined the creep response of nickel base C263 superalloy at 800°C subsequent to room temperature pretension. The results show that the minimum creep rate can be slightly enhanced with increasing amount of prestrain. More recently, similar trends are reported in [18] where the creep response of polycrystalline copper at 100°C is enhanced by increasing amount of precompression.

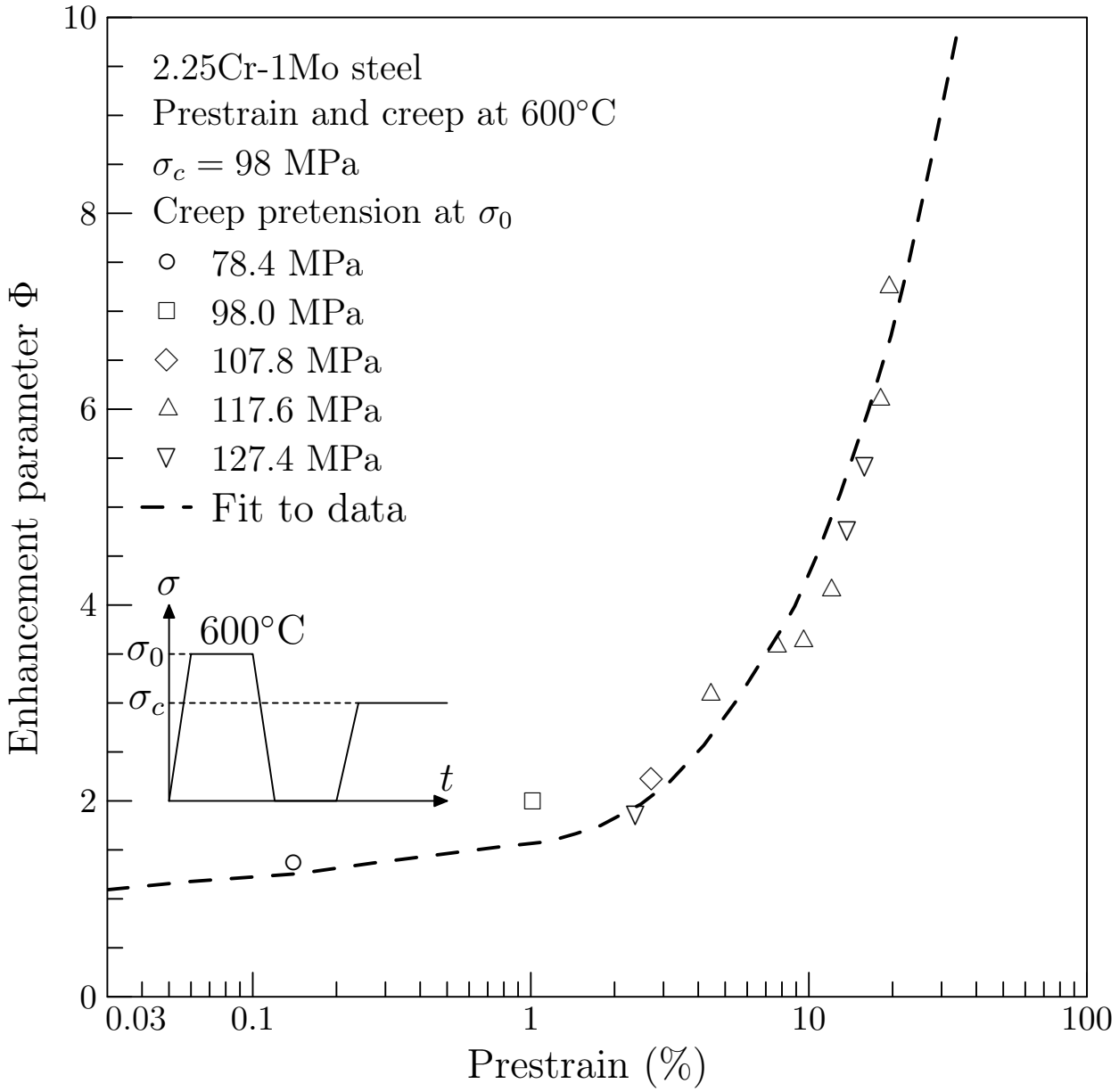

Figure 10: Creep enhancement as a function of amount of prestrain in creep test of 2.25Cr-1Mo ferritic steel at 600°C (Adapted from [13]).

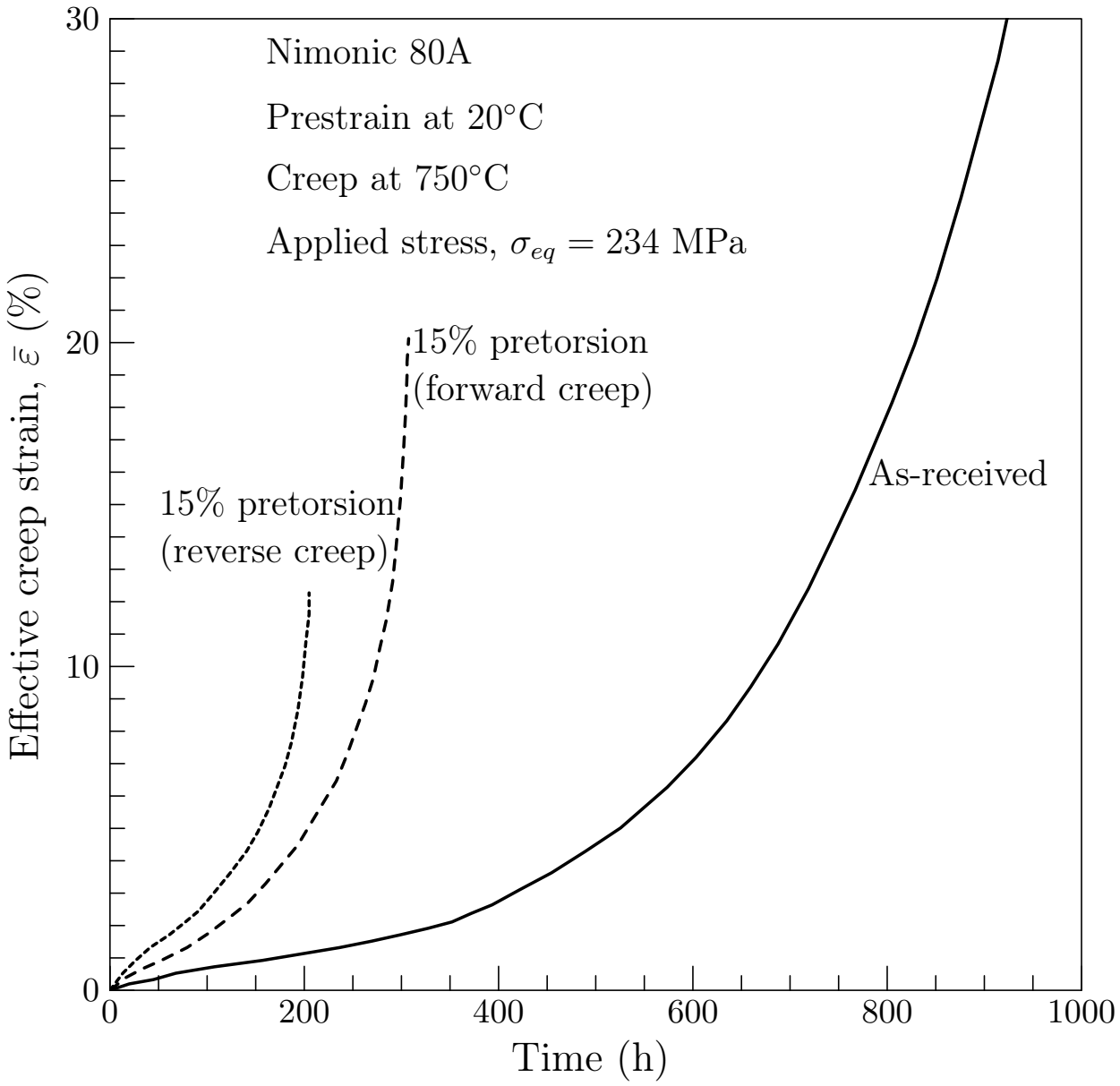

Figure 11: Torsion creep curves at 750°C and a equivalent stress of 300 MPa for Nimonic 80A (Adapted from [14]).

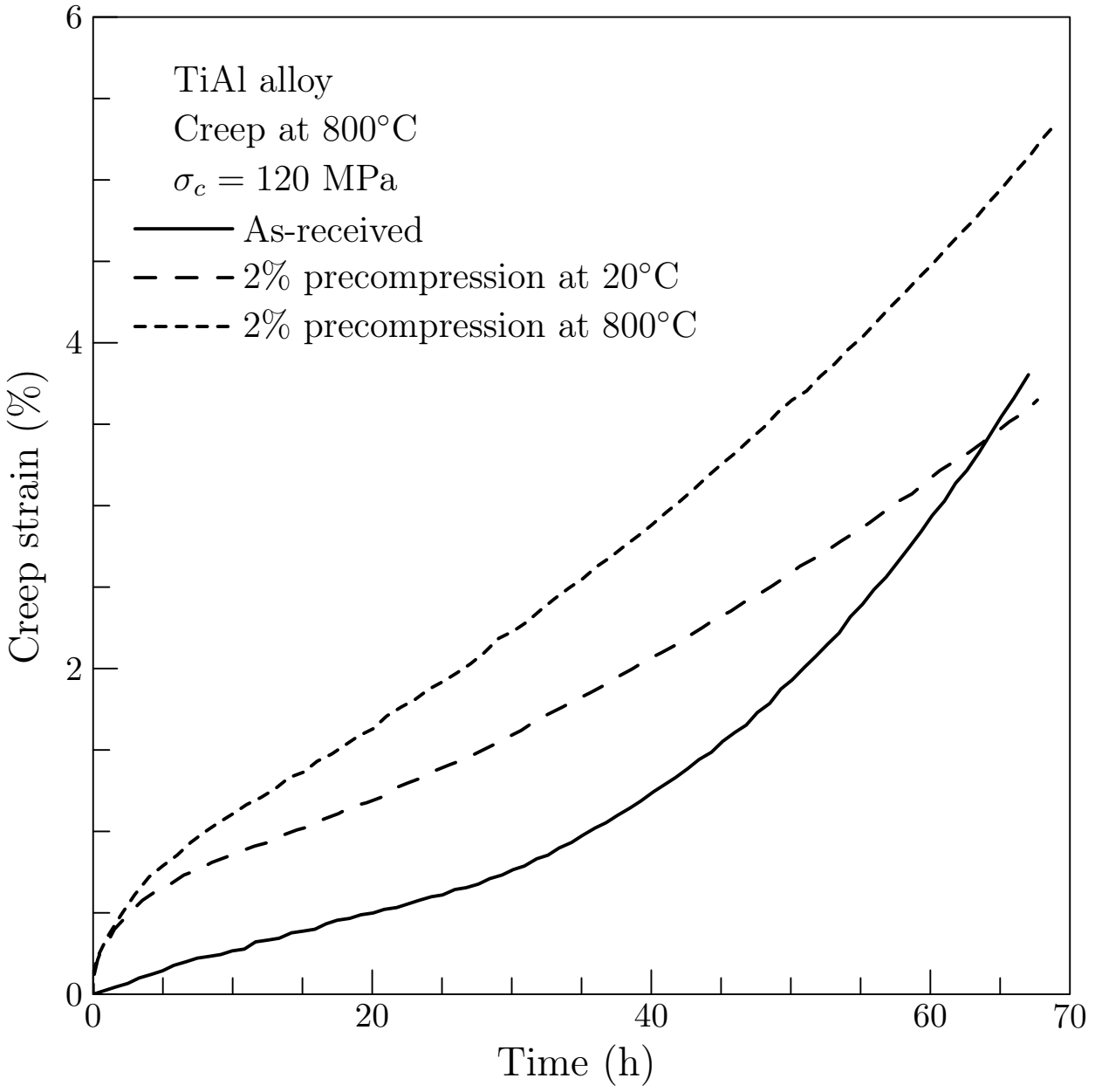

Figure 12: Creep curves at 800°C and 120 MPa for polycrystalline TiAl alloy as-received and after prior deformation by 2% at room temperature and 800°C (Adapted from [17]).

2.3 Effects on creep fracture

In addition to the influence on creep deformation, prior deformation may also affect the creep fracture behaviour by changing creep ductility and creep life.

A common way to describe creep fracture behaviour in uniaxial tension is the Monkman-Grant relation [19] which considers an inverse dependence of the creep rupture life t_f on the minimum creep rate $\dot{\varepsilon}_m$

$$(\dot{\varepsilon}_m)^k t_f = M, \tag{4}$$

where k, M are constants dependent on temperature and material and the constant M is known as the Monkman-Grant constant. To quantify the contributions of prestrain to creep fracture behaviour, the Monkman-Grant relation (Eq. 4) for as-received and prestrained 2.25Cr-1Mo steels was examined in [13] by Tai and Endo and the results are shown in Fig. 13. It is found that despite the slight scatter of results the Monkman-Grant rule holds ($k = 0.772$ and $M = 27.4$) and appears to be insensitive to prestrain. The prestrain values corresponding to individual data points in Fig. 13 were not provided in [13]. Thus, the dependence of creep ductility on prestrain for these data cannot be directly identified. However, as the data in Fig. 13 show a weak dependence of the Monkman-Grant parameters on pre-strain, it is reasonable to conclude that for this material the creep ductility is not strongly sensitive to pre-strain under the conditions examined.

The levels of pre-strain examined by [13] and shown in Fig. 10 and Fig. 13 are high, (up to 19.4%). There is insufficient information in [13] to allow an estimate of the creep ductility of a particular prestrained specimen. However, from Fig. 13 the maximum creep ductility (estimated by multiplication of minimum creep rate and creep life) of the as-received specimens is approx. 20% with the lowest measured creep ductility approx. 2%. As seen in Fig. 10, the creep-prestrain level ranges from 0.14% to 19.4% (only two specimens are lower than 1%). Therefore, some prestrained specimens in Fig. 10 and Fig. 13 may have been close to failure

Willis et al. [20] examined the effect of prestrain on the subsequent creep fracture behavior of PST 316H stainless steel at 575°C and under a constant stress of 450 MPa using uniaxial creep specimens. Rupture ductility in terms of creep strain at failure was found to reduce with increasing prestrain level, while rupture life was found to be weakly dependent on prestrain level. To allow comparison with other data in this section, the creep ductility data of [20] are presented in Fig. 14 in terms of the Monkman-Grant relation. It is seen that the Monkman-Grant constant is relatively insensitive to pre-strain for prestrains below 20%, while for prestrain larger than 20% a reduction in the Monkman-Grant constant is observed. The contrast in the trend for creep ductility in [20] (observed dependence on prestrain) and Monkman-Grant parameters (lack of dependence on prestrain for prestrain $< 20\%$) may be due to difficulties in identifying the failure strain in a creep test or due to the experimental data scatter caused by microstructural variability of this particular material. Note also that the data in [20] are for short-term tests with a creep life less than 100 hours. Long term data for this particular material (PST 316H) are not readily available in the open literature. Based on the data reviewed in this article for similar materials, prestrain (less than 20%) may reduce the Monkman-Grant constant under long-term creep test conditions for the PST

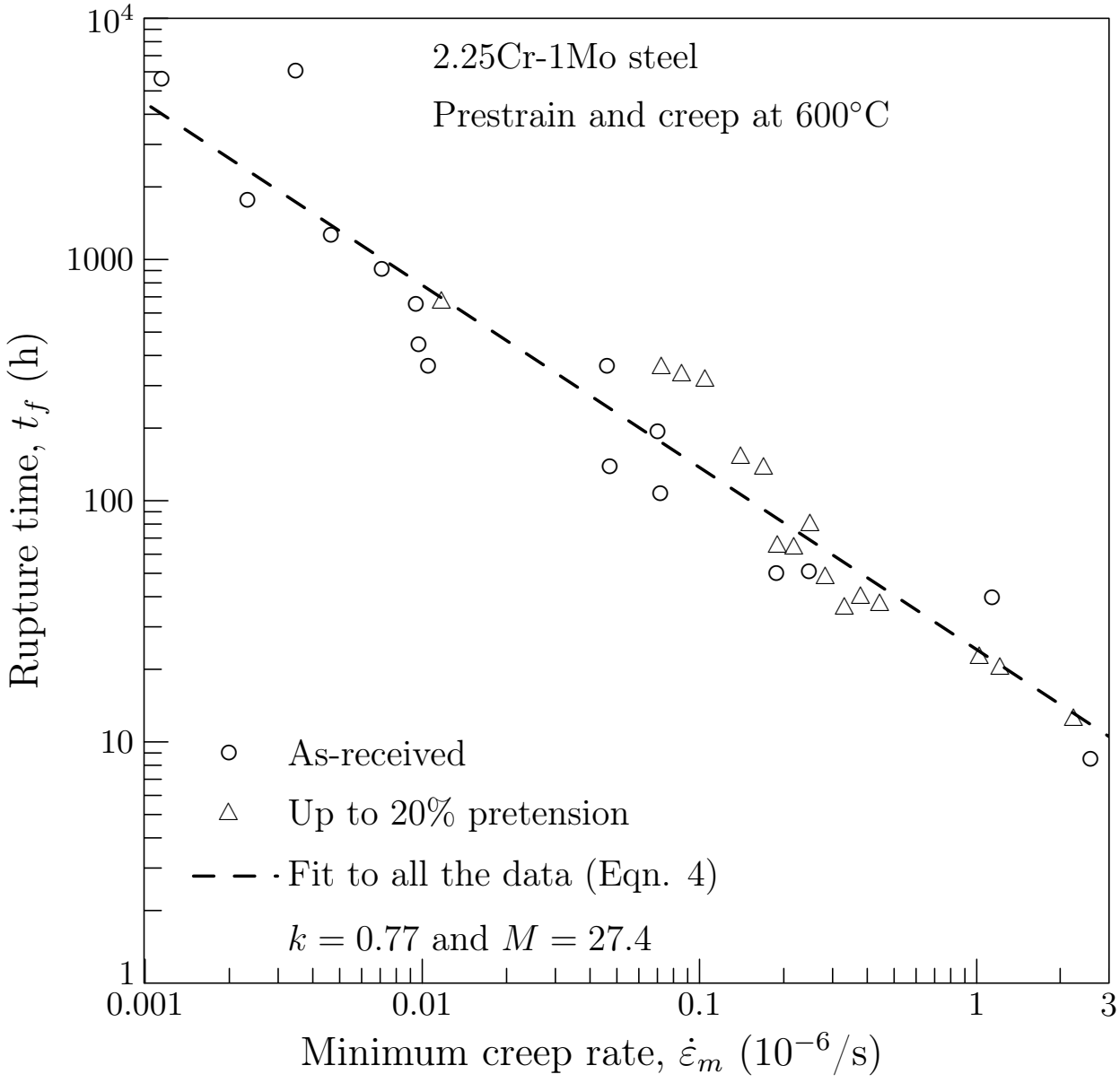

Figure 13: Monkman-Grant relation incorporating as-received and prestrained 2.25Cr-1Mo steels (Adapted from [13]).

316H material.

Wilshire and Willis [2] examined FST 316H stainless steels as a supplement to the results in [20]. As seen in Figs. 7 and 8 rupture ductility decreases while rupture life increases with prestrain for this material. Figure 15 shows the variations of Monkman-Grant relation caused by different amount of prestrain at room temperature. It is seen that the Monkman-Grant constant of specimens prestrained by 17% at room temperature is less than that of as-received specimens, consistent with the data of [20]. For specimens with a prestrain of 12% there is a transition of the Monkman-Grant constant from that of the as-received material at higher creep rates ($\dot{\varepsilon}_m > 0.02 \times 10^{-6}$) to that of specimens prestrained by 17% at lower creep rates ($\dot{\varepsilon}_m < 0.005 \times 10^{-6}$). The transition is indicated by the line linking the two parallel lines in Fig. 15.

Auzoux et al. [21] examined the effect of prestrain on the subsequent creep fracture behavior of 316L(N) austenitic stainless steel at 600°C, using as-received and prestrained cylindrical specimens (20 mm gauge length; 4 mm diameter). For these specimens, prestrain was imposed by rolling between 400°C and 600°C to reduce the thickness by $15 \pm 0.4\%$. Figure 16 shows the Monkman-Grant plots for as-received and prestrained materials, indicating a significant reduction in the Monkman-Grant ductility.

Davies et al. [11] studied the effect of precompression on creep fracture of 316H stainless steels. Figure 9 shows that both rupture ductility and rupture life are reduced with increasing prestrain. Consistent with this observation, a significant reduction in the Monkman-Grant constant can be identified for the prestrained specimens as seen in Fig. 17.

For non-ferrous materials, the effect of prior deformation on creep rupture life of Nimonic 80A was examined in [14]. Figure 11 shows that prestrain (under pretension and pretorsion) reduces both rupture ductility and rupture life. Insufficient data are provided in [14] to allow the application of the Monkman-Grant relation to be examined for this material. Figure 18 shows that the creep rupture lives of prestrained specimens are significantly lower than those of as-received specimens at the same stress level. It may also be noted that 'reverse creep' leads to a larger reduction in creep rupture life than 'forward creep'.

The pretension effect on subsequent creep fracture at 750°C for astroloy was investigated in [22]. A flat tensile specimen was deformed plastically at room temperature to a prestrain of 10%, and two sets of creep specimens were extracted with long axes parallel and perpendicular to the prestrain direction, respectively (gauge length 2 mm; width 1.5 mm; thickness 0.7 mm). For comparison, non-prestrained creep specimen were also tested (gauge length 14 mm; width 6.5 mm; thickness 1.5 mm). Figure 19 shows the comparison of creep rupture time as a function of applied stress. It is observed that pretension results in a reduction in creep rupture time particularly when the creep loading direction is perpendicular to the prestrain direction.

Prestrain effects on creep crack growth have also been examined using notched specimens. Worswick and Pilkington [23] examined the effect of high temperature (666°C) prestrain (tension) on subsequent creep crack growth for a 0.5Cr-0.5Mo ferritic steel at 550°C, using three point bending specimens (152 mm × 18.75 mm × 12 mm) with a notch (fatigue-cracked to approx. 1/3 of width). The macroscopic creep crack growth rate, $\dot{a}$, was described in terms

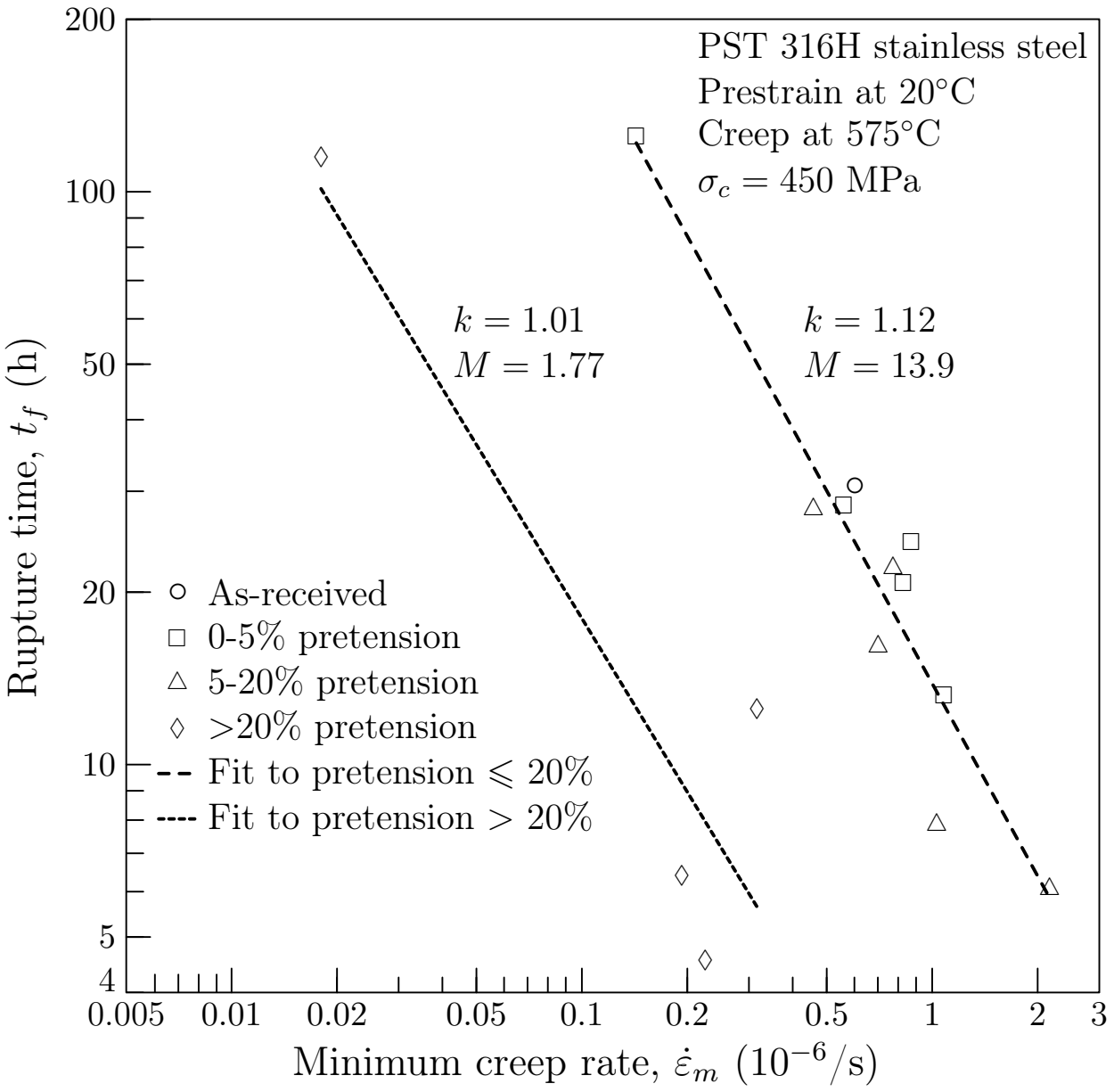

Figure 14: Monkman-Grant relation incorporating as-received and prestrained PST 316H stainless steels (Data from [20]).

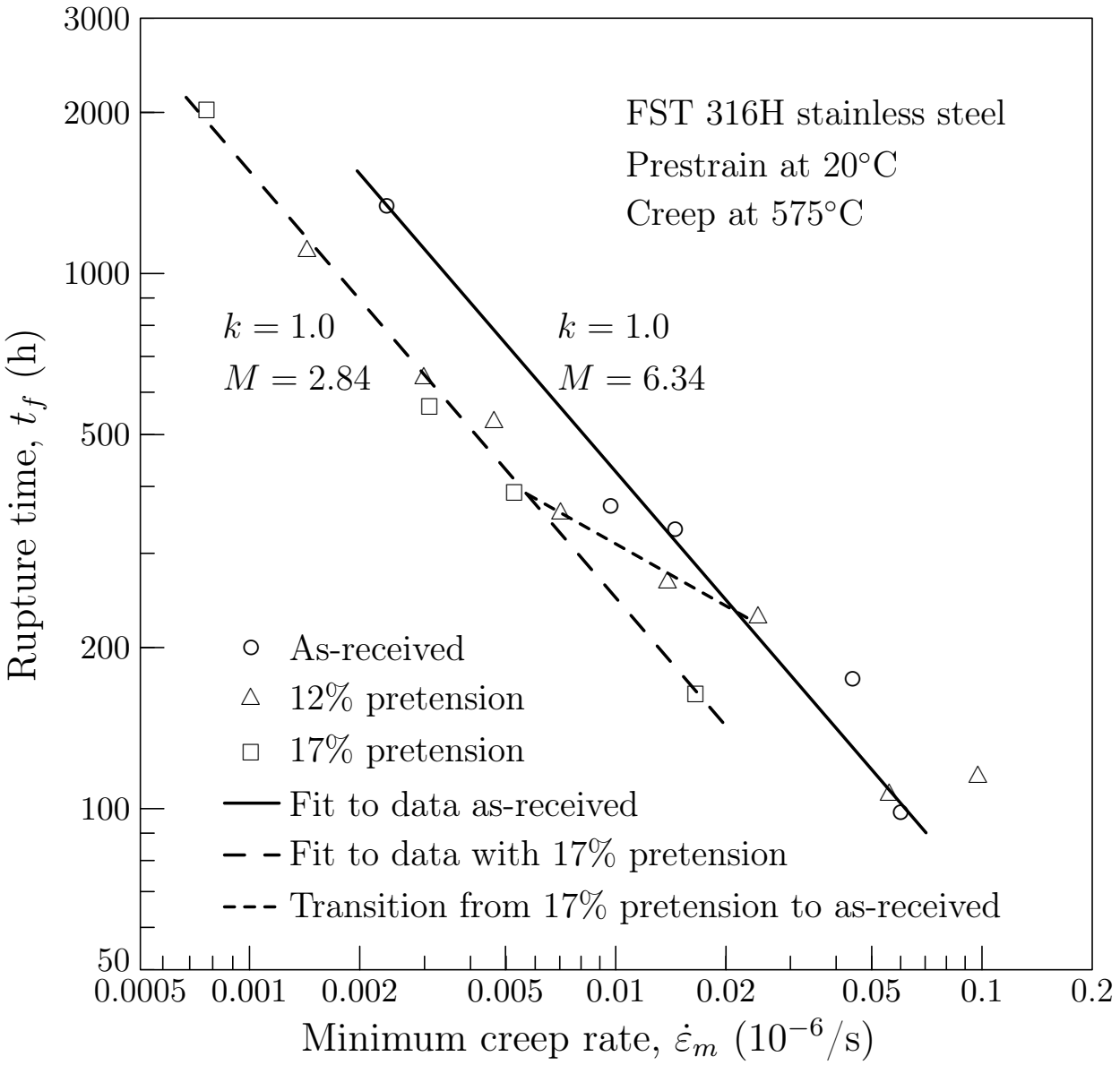

Figure 15: Monkman-Grant relation incorporating as-received and prestrained FST 316H stainless steels (Adapted from [2]).

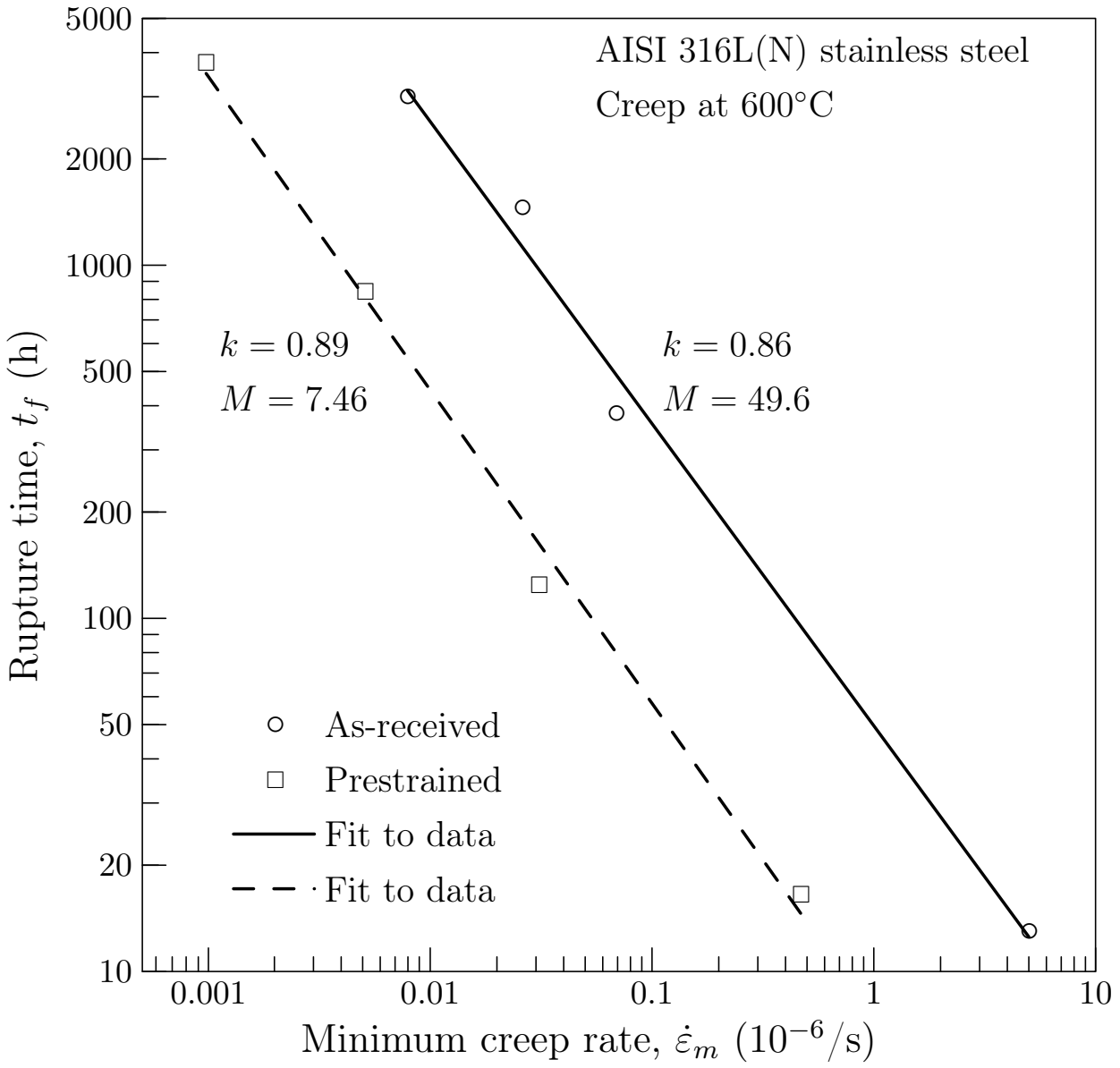

Figure 16: Prestraining effects on high temperature (600°C) creep fracture behavior for smooth cylindrical specimens (Data from [21]).

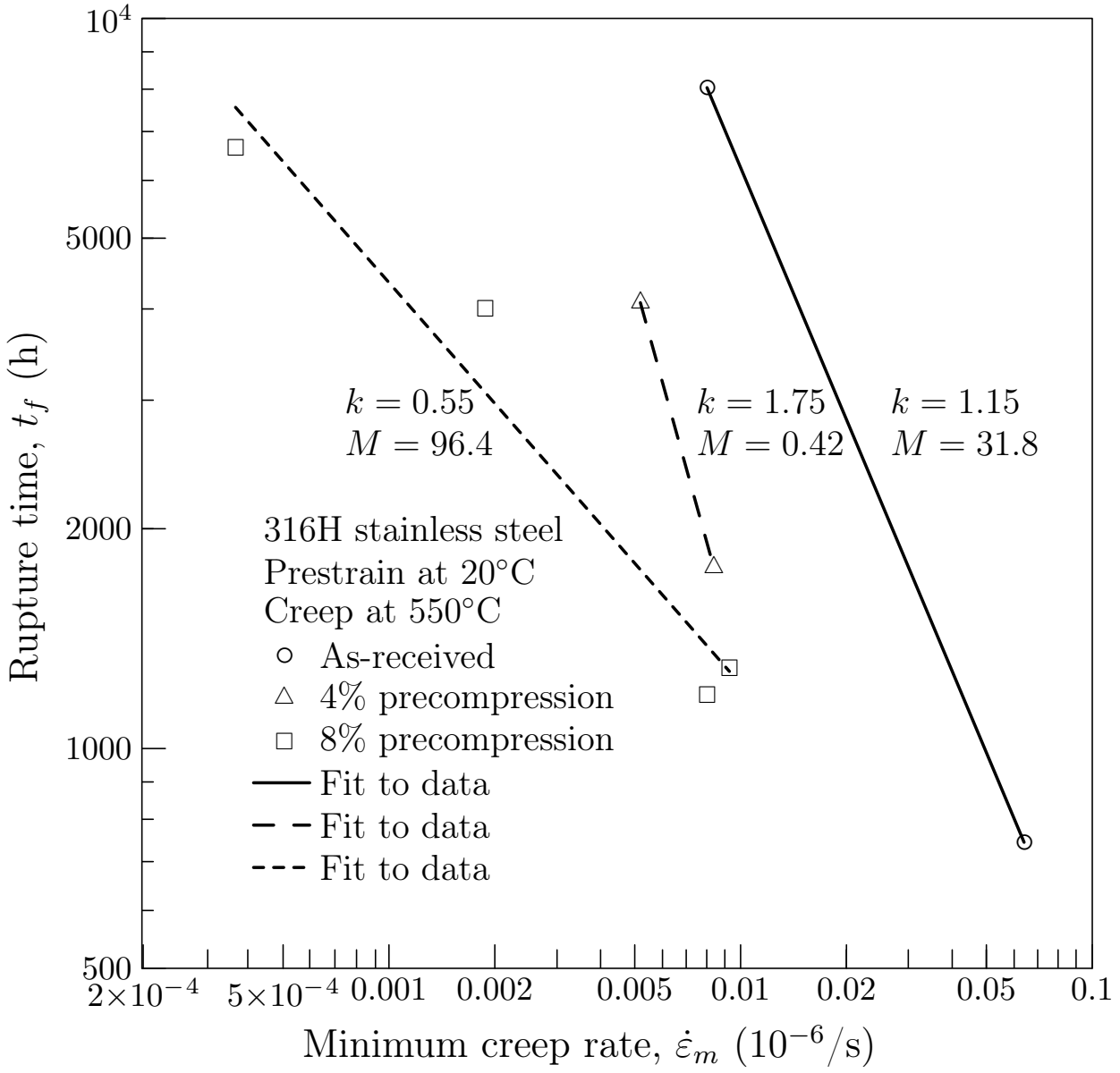

Figure 17: Precompression effects on high temperature (550°C) creep fracture behavior for 316H stainless steel (Data from [11]).

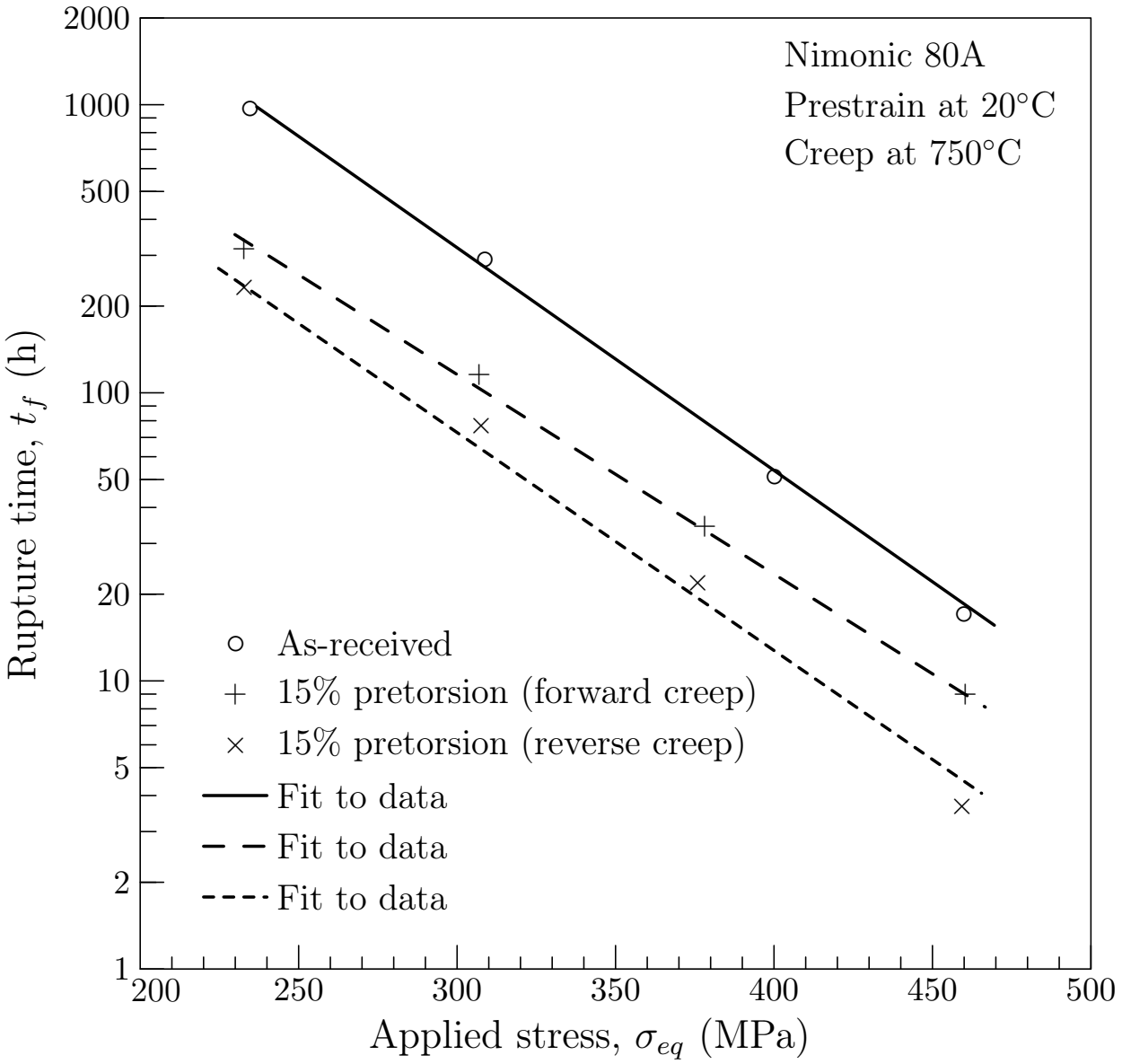

Figure 18: Time to fracture against effective stress for torsion creep tests of Nimonic 80A (Adapted from [14]).

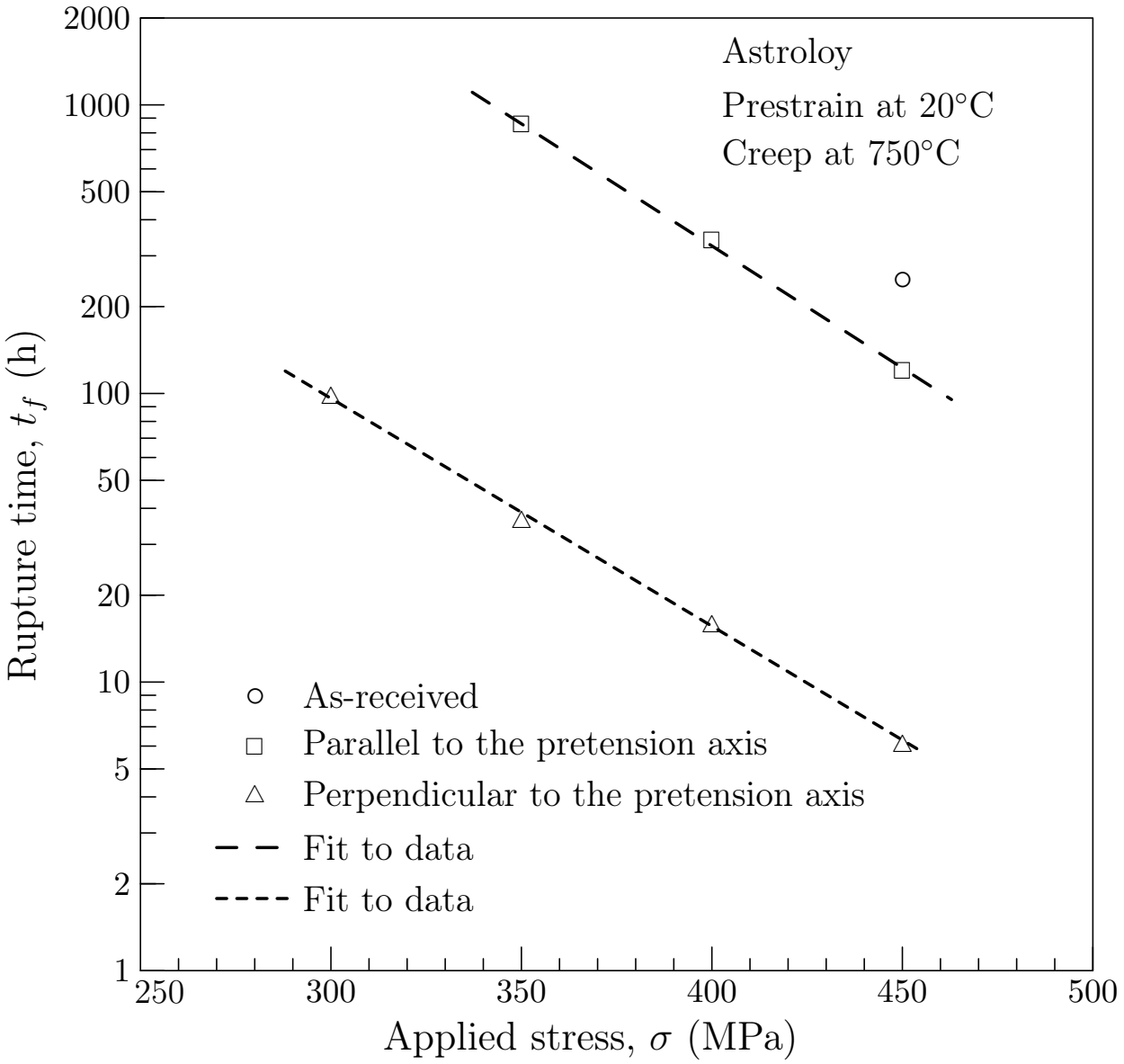

Figure 19: Time to fracture against effective stress for tensile creep tests of Astroloy (Adapted from [22]).

of the stress intensity factor, K, by

$$\dot{a} = AK^n, \tag{5}$$

where A and n are constants (see, e.g., [24]). Figure 20 shows the results for as-received and prestrained materials. It can be seen that the specimens with prestrain of 0.26% show similar fracture behaviour to the as-received materials. However a prestrain of 0.58% leads to a significant increase in the crack growth rate.

3 Microstructural effects of prior inelastic deformation

Creep deformation mechanisms can be categorised into the following modes (see, e.g., [1]): (i) dislocation glide at high stress level which involves dislocation moving along slip planes and overcoming obstacles aided by thermal activation; (ii) dislocation creep at intermediate stress levels which involves dislocation movement overcoming barriers by vacancy diffusion and (iii) diffusion creep at low stress levels which is controlled by stress-controlled atomic diffusion. In addition, for polycrystalline materials grain-boundary sliding may play an important role in initiating intergranular fracture during creep, although it does not contribute significantly to steady-state creep. It is expected that any microstructural change in a material resulting from prior deformation will affect the subsequent creep response and fracture behaviour at high temperature. In this Section, attention is focused on the microstructural changes caused by prior deformation and on examining their contribution to subsequent high temperature creep.

3.1 Effects on dislocation substructure

A useful starting point to consider the effect of microstructural changes on creep response is the Orowan equation (see, e.g., [25])

$$\dot{\varepsilon} = \rho_m b v, \tag{6}$$

where ρ_m indicates mobile dislocation density, b is the Burger's vector length and v is the average velocity of the dislocations.

Many authors (see, e.g., [2, 7, 10, 26–29]) have pointed out that dislocation density, ρ increases rapidly with increasing plastic strain. The increased dislocation density introduced by prestraining at room temperature cannot be fully recovered during the subsequent heating process prior to creep and may create strong barrier to dislocation movement during creep. Thus, the dislocation velocity in the Orowan equation is reduced, without increasing the mobile dislocation density, leading to a reduction in creep strain rate. However, prestrain may not always lead to an increase in creep resistance as observed in [3, 13, 17, 18]. In this case, as argued in [3, 17], dislocations introduced during prestraining may remain mobile thus leading to an increase in the strain rate (creep enhancement effect) through an increase in ρ_m in Eq. (6).

In addition to the contribution to dislocation density, prior deformation at room temperature can also introduce important effects on lattice structure near grain boundaries. For example, Li et al. [18] reported that prior deformation is prone to producing high angle

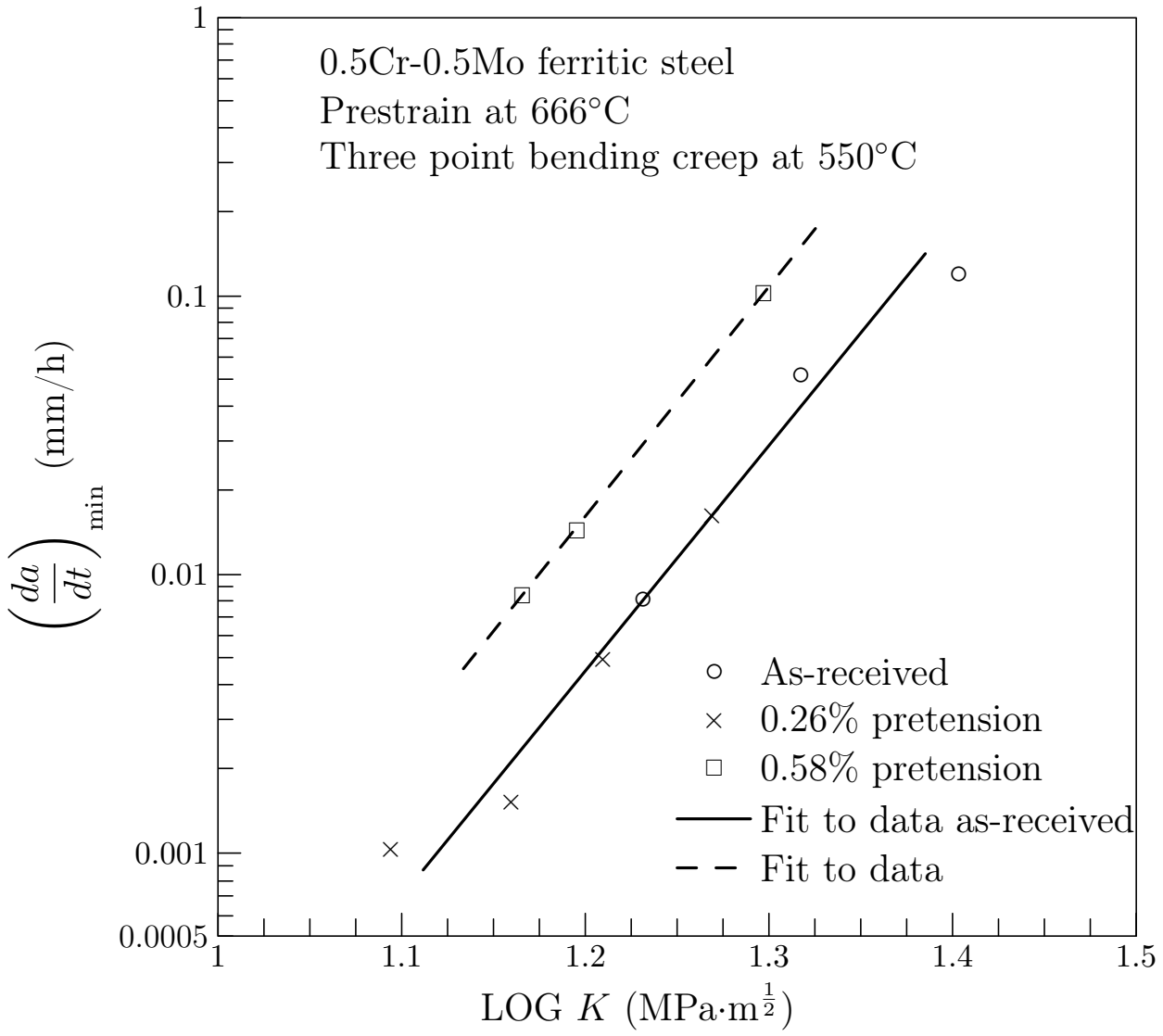

Figure 20: High temperature pretension effects on the subsequent creep crack growth. (Adapted from [23]).

boundaries for polycrystalline copper. Typically two competing effects can be introduced by high-angle grain boundaries. Firstly, they can improve the rate of generation of dislocations resulting in material hardening due to dislocation entanglements (resistance). Secondly, they can improve the dislocation-annihilation rate by fast climb of edge dislocations in dipole configuration via grain boundary diffusion to soften the material (enhancement). Li et al. [18] found for a sufficiently small spacing of high-angle boundaries, the softening effect may become dominant, and consequently lead to a drop in creep resistance at high temperature (creep enhancement effect). For prior deformation at high temperature, it is believed that in some cases dislocation substructures are preserved such that dislocation motion in subsequent creep is restricted, leading to a resistance effect on subsequent creep, as shown in [2]. However, this assumption cannot explain the temperature dependence of the prestrain effect, observed in [5, 10, 17] for 304 stainless steel, polycrystalline Ti-52Al and single-crystal Ni_3Al, respectively, where the same amounts of prestrain at room and high temperatures can exert different effects on subsequent creep. Kikuchi and Ilschner [5] postulated that the temperature effect shown in Fig. 4 is due to high temperature dynamic strain aging which leads to a maximum work hardening rate in the temperature range of $300 - 650°C$ thus a higher resistance effect when prestrain occurs at these temperatures. Cairney et al. [10] suggested that the temperature effect may be due to the different dislocation structures induced by prestraining at room and high temperature. They found that specimens prestrained at 520°C have shorter length of Kear-Wilsdorf (KW) locks than specimens prestrained at room temperature, therefore allowing the source of dislocations to operate differently, resulting in a larger resistance effect than that of prestrain at room temperature.

3.2 Influence on void nucleation and distribution

In addition to exerting significant influence on dislocation structures, prior deformation can also lead to microstructural degradation by producing cavities or micro-cracks within materials and accordingly affect the subsequent high temperature creep and creep fracture behaviour. In this section, we focus on prior deformation at room temperature since cavity nucleation is less likely to occur by prestrain at high temperature due to high dislocation mobility (see, e.g., [30]).

To assess the influence of prior deformation on grain boundary cavity nucleation and distribution, the cavity density by transmission electron microscope (TEM) after prior deformation was measured in [14]. Figure 21 shows the cavity density as a function of strain. The cavity density, here, was defined as

$$\rho_c = \frac{n_c}{t - d} \tag{7}$$

where n_c is the number of cavities observed in a unit foil area of thickness, t, and d the mean diameter of cavities. Figure 21 shows that the cavity density depends strongly on the value of strain and with increasing strain the number of cavities per unit volume increases.

The nucleation mechanisms of cavities for prestrained astroloy were examined in [22]. It was found that prestrain tends to result in grain boundary damage in terms of microcracking at the interface between carbide (primarily $M_{23}C_6$) and matrix. In addition, the

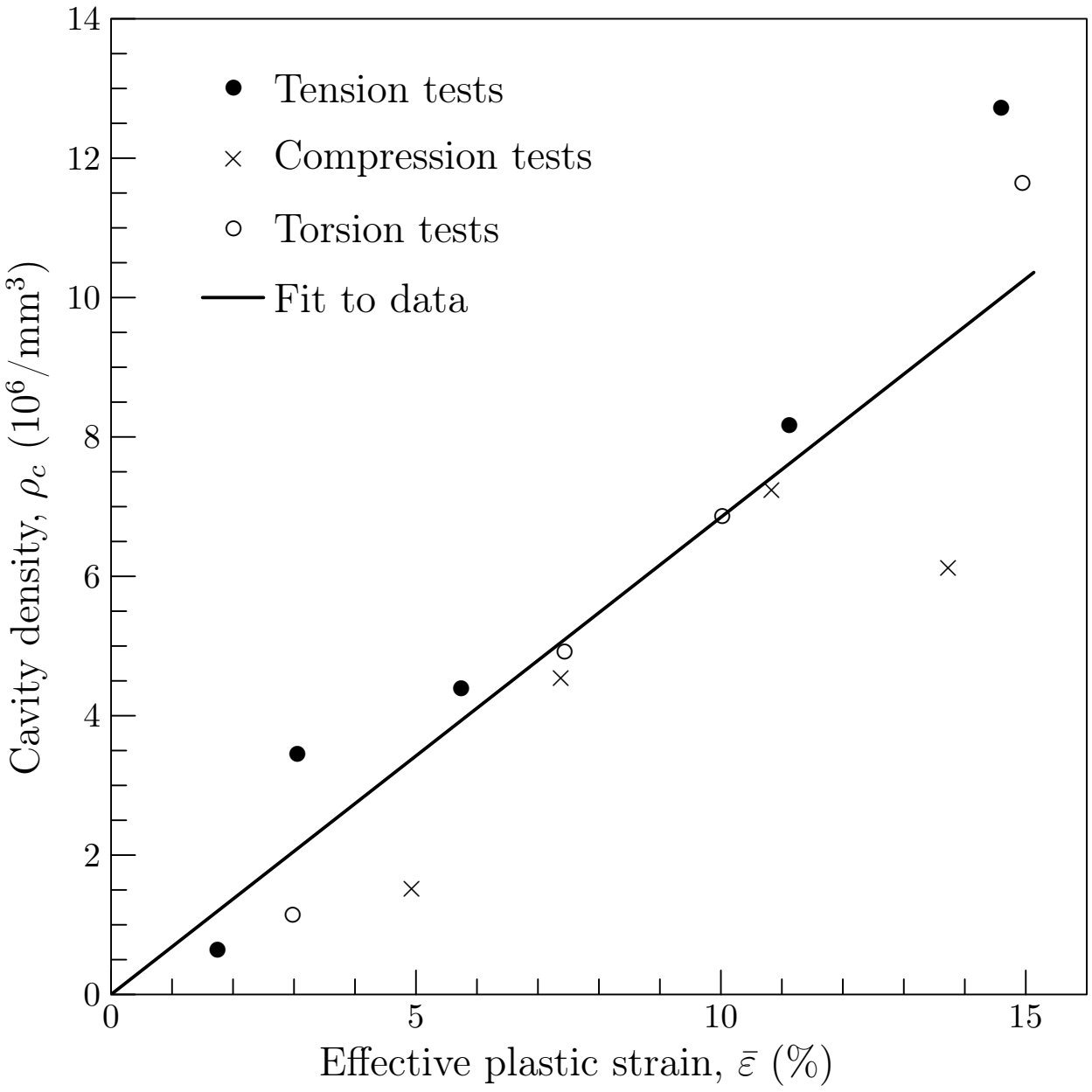

Figure 21: Variation of number of cavities per unit volume with effective plastic strain (Adapted from [14]).

local residual stress within grains developed by prestraining at room temperature was found to alter significantly the subsequent creep fracture behaviour resulting in an anisotropic creep response. Following a simplified theoretical model of an elliptical inclusion in an isotropic homogeneous elastic matrix (e.g., [31]),the residual stress distribution near an inclusion was calculated in [22] and it was postulated that the residual stress introduced near the inclusion by prestrain plays a key role in subsequent (anisotropic) creep behaviour. Thus, prior deformation has been proposed as a mechanism for subsequent creep enhancing effects (and anisotropic behaviour) through the introduction of cavities or significant residual stress near grain boundaries. However, evidence for this interpretation is not strong and further investigations are required to provide more evidence to support these postulations. In addition, the underlying microstructural mechanisms for the reduction in the Monkman-Grant ductility caused by prior deformation as shown in Figs. 13, 14, 15, 16 and 17 are not clear.

4 Modelling studies of prestrain effects

In order to quantify the creep behaviour of materials accounting for prior deformation, constitutive models have relied primarily on phenomenological approaches. In this section, we focus on these models to predict the effect of prior deformation on the subsequent creep.

An empirical model was proposed in [32] to describe the dependence of creep strain rate $\dot{\varepsilon}$ on prior creep strain, ε_p, for a 2.25Cr-Mo steel. The model is essentially a modification to a Norton law for creep and may be written as

$$\dot{\varepsilon} = A_0 \exp\left(m\varepsilon_p + s\varepsilon - \frac{Q_0}{RT}\right)\sigma_c^n, \tag{8}$$

where A_0 is a constant, m depends only on prestrain temperature and stress (for the material examined $m = 10 \pm 0.4$), s is a constant which depends on stress and temperature, σ_c is the applied stress during creep, n is the creep stress exponent (for the material examined $n = 9.7 \pm 0.2$), Q_0 is the apparent activation energy for creep, R is the Boltzmann constant and T is the absolute temperature. Equation 8 reveals that for given temperature and stress, the creep rate at a fixed level of creep strain increases with increasing prestrain. However, this empirical model was developed only for uniaxial creep deformation with prestrain effect. No extension to multi-axial creep deformation was presented.

Murakami et al. [33] proposed a numerical scheme to investigate coupled plastic and creep damage. They assumed that the plastic damage and subsequent creep damage occur at grain boundaries through cavity growth and the overall damage can be interpreted as an internal state variable representing the area density of the cavities. The damage state is then expressed as a sum of plastic damage and creep damage as follows:

$$\mathbf{\Omega} = \mathbf{\Omega}_P + \mathbf{\Omega}_C, \tag{9}$$

where $\mathbf{\Omega}$ is a symmetric damage tensor interpreted as an internal variable representing the area density of grain boundary cavities, and $\mathbf{\Omega}_P$ and $\mathbf{\Omega}_C$ indicate plastic and creep damage

tensors, respectively. To take into account the stress magnification by internal damage, a net stress tensor, $\mathbf{S}$ is introduced and given by

$$\mathbf{S} = \mathbf{\Phi}\boldsymbol{\sigma}, \tag{10}$$

where

$$\mathbf{\Phi} = (\mathbf{I} - \mathbf{\Omega})^{-1} \tag{11}$$

which defines the amplitude of the magnification of the Cauchy stess $\boldsymbol{\sigma}$. Based on the experimental data in [14] for Nimonic 80A which showed the cavities due to prior deformation at room temperature are mainly developed on grain boundaries parallel to the principal stress direction, the plastic damage tensor $\mathbf{\Omega}_P$ was specified as

$$\mathbf{\Omega}_P = \gamma_P \mathbf{I} + \sum_{i=1}^{3} \mathbf{M}_{P(i)} : \left[\boldsymbol{\nu}_{P(i)} \otimes \boldsymbol{\nu}_{P(i)}\right], \tag{12}$$

where γ_P and $\mathbf{M}_{P(i)}$ are a scalar function and a fourth order tension function of the prior plastic strain tensor $\boldsymbol{\epsilon}_P$, respectively, the symbols $\boldsymbol{\nu}_{P(i)}$ and $\mathbf{I}$ indicate the principal plastic strain directions and the unit tensor, respectively, and : and $\otimes$ denote the double contraction and the tensorial product, respectively. Finally, the creep rate is assumed to be governed by Norton's law as

$$\dot{\boldsymbol{\epsilon}}_C = \frac{3}{2} A \left(S_{eq}\right)^{n-1} \mathbf{S}_d, \tag{13}$$

where S_{eq} is the equivalent net stress with

$$S_{eq} = \sqrt{\frac{3}{2} \mathrm{tr}\left(\mathbf{S}_d^2\right)}, \tag{14}$$

$\mathbf{S}_d$ the deviatoric part of $\mathbf{S}$, and A and n are material constants. To quantify the evolution of creep damage, $\mathbf{\Omega}_C$, based on metallurgical observations on creep damage processes (see, e.g., [34]), it was assumed in [33] that creep damage is characterised by the formation of plane cavities on the grain boundaries perpendicular to the maximum principal stress direction. The creep damage tensor is governed by

$$\dot{\mathbf{\Omega}}_C = B \left[\zeta S_{(1)} + (1-\zeta) S_{eq}\right]^k \left[\mathrm{tr}\left(\mathbf{\Phi}\left(\boldsymbol{\nu}_{C(1)} \otimes \boldsymbol{\nu}_{C(1)}\right)\right)\right]^l \left[\boldsymbol{\nu}_{C(1)} \otimes \boldsymbol{\nu}_{C(1)}\right], \tag{15}$$

where B, k, ζ and l are material constants; $S_{(1)}$ and $\boldsymbol{\nu}_{C(1)}$ denote the maximum principal stress and corresponding direction of $\mathbf{S}$, respectively. Noting Eqs (9), (11) and (12), it is found that $\mathbf{\Phi}$ can be seen as a function of the creep damage tensor $\mathbf{\Omega}_C$ and the prior plastic strain tensor $\boldsymbol{\epsilon}_P$. Therefore Eq. (15) provides a nonlinear differential equation with respect to the creep damage tensor $\mathbf{\Omega}_C$ and takes prior plastic deformation into account. Using this phenomenological model, reasonable agreement with the data in [14] for Nimonic 80A was obtained in [33]. Figure 22 shows the comparisons between modelling and experimental results. Note that in [33] prior deformation is seen as a factor introducing damage. Therefore only the enhancing effect of prior deformation on creep discussed in Section 2.2 can be

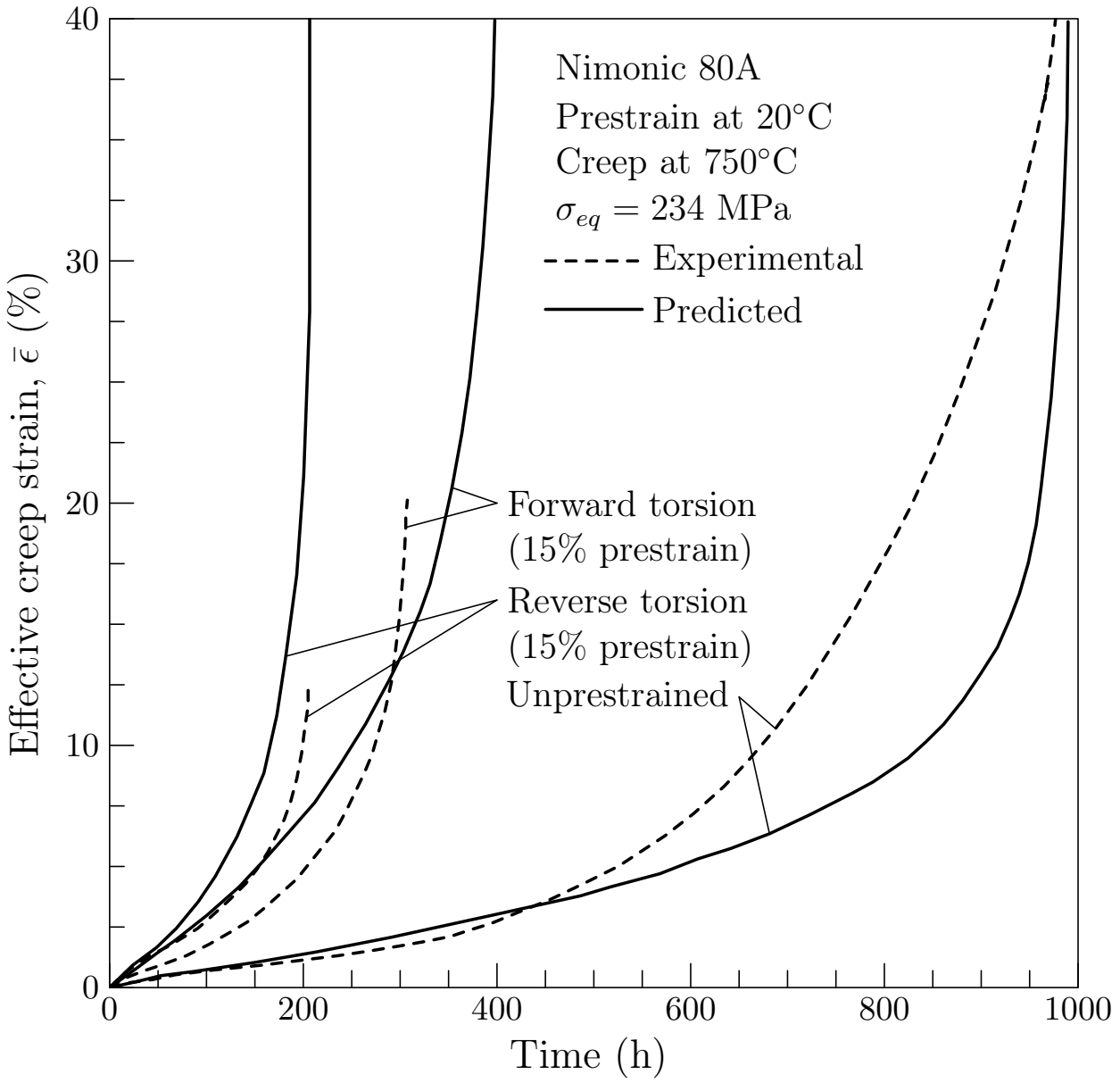

Figure 22: Torsion creep curves after pretorsion at room temperature for Nimonic 80A at 750°C where experimental and predicted curves are adapted from [14] and [33], respectively.

predicted, although in many cases prior deformation has been reported to cause resistance effects as discussed in Section 2.1. Next we will discuss the phenomenological models which can predict creep resistance due to prior deformation.

Xia and Ellyin [35] proposed a rate-dependent inelastic constitutive model to study the creep deformation including the prior plastic strain effect. In this study, rather than Eq. (10) given in [33], a net stress tensor $\mathbf{S}$ is written as

$$\mathbf{S} = \boldsymbol{\sigma} - \boldsymbol{\alpha}, \tag{16}$$

where $\boldsymbol{\alpha}$ is an internal tensor variable (called "internal stress", "equilibrium stress", "back stress" or "rest stress" in the literature). As in [33] Norton's law, Eq. (13), is used in [35] and the evolution of $\boldsymbol{\alpha}$ during creep is governed by

$$\boldsymbol{\alpha} = (\alpha_P + \alpha_C)\,\frac{\boldsymbol{\sigma}_d}{\sigma_{eq}}\left(1 - Ce^{-\beta\bar{\epsilon}_C}\right), \tag{17}$$

where β and α_C are material constants, α_P is related to prior plastic strain, $\boldsymbol{\sigma}_d$ and σ_{eq} denote the deviatoric and von Mises equivalent stress, respectively, $\bar{\epsilon}_C$ is effective creep strain, and C is an integration constant related to plastic prestrain. Furthermore, the parameters α_P and C which depend on plastic prestrain are postulated to be of a specified form based on the experimental results in [4]. The material constants are obtained in [35] from creep data without prestraining, and the creep resistance effect of prestrain is predicted in good agreement with experimental results. Figure 23 shows the comparisons for torsion creep tests of prestrained specimens.

Note that in the models [33, 35] the temperature effect is not taken into account. Therefore, the dependence of material parameters on temperature in these models must be correlated with experimental data at different temperatures.

Peleshko [36] re-examined creep theory for bodies with anisotropy due to plastic prestrain using deformation theory rather than flow theory (e.g., [33, 35]). Peleshko [36] assumed there are no additional plastic strains during creep, and decomposed the total strain into three parts given by

$$\boldsymbol{\epsilon} = \boldsymbol{\epsilon}_p + \boldsymbol{\epsilon}_e + \boldsymbol{\epsilon}_c, \tag{18}$$

where $\boldsymbol{\epsilon}_p$, $\boldsymbol{\epsilon}_e$ and $\boldsymbol{\epsilon}_c$ denote prestrain, elastic strain and creep strain, respectively. The prestrain $\boldsymbol{\epsilon}_p$ is introduced in a single load/unload cycle up to stress $\boldsymbol{\sigma}_0$ (with a deviatoric part $\boldsymbol{\sigma}_{0d}$). The creep strain $\boldsymbol{\epsilon}_c$ is introduced by applied stress $\boldsymbol{\sigma}_c$ (with a deviatoric part $\boldsymbol{\sigma}_d$).

Starting from the assumption that the creep strain vector $\boldsymbol{\epsilon}_c$ lies in the plane linearly spanned by $\boldsymbol{\sigma}_d$ and $\boldsymbol{\sigma}_{0d}$ in deviatoric stress space, the anisotropic creep response is written as

$$\boldsymbol{\epsilon}_c = \Psi_1 \frac{\boldsymbol{\sigma}_d}{\sigma_{eq}} + \Psi_2 \frac{\boldsymbol{\sigma}_{0d}}{(\sigma_0)_{eq}}, \tag{19}$$

where σ_{eq} and $(\sigma_0)_{eq}$ denote von Mises equivalent stresses corresponding to $\boldsymbol{\sigma}_c$ and $\boldsymbol{\sigma}_0$, respectively, and the functions Ψ_1 and Ψ_2 have the following form

$$\Psi_1 = \Psi_1\left(t, \sigma_{eq}, (\sigma_0)_{eq}, \boldsymbol{\sigma}_{0d} : \boldsymbol{\sigma}_d\right), \tag{20a}$$

$$\Psi_2 = \Psi_2\left(t, \sigma_{eq}, (\sigma_0)_{eq}, \boldsymbol{\sigma}_{0d} : \boldsymbol{\sigma}_d\right), \tag{20b}$$

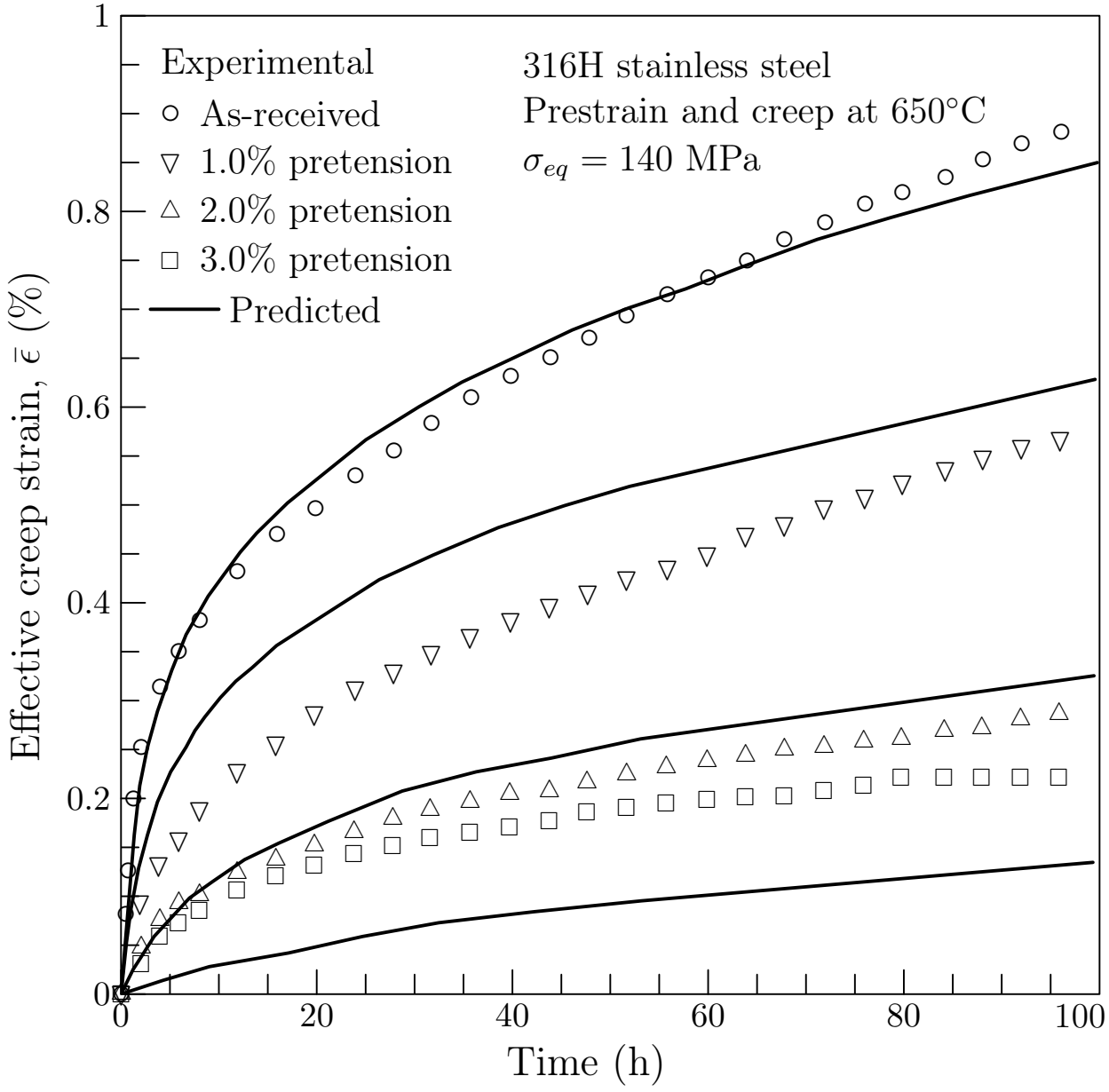

Figure 23: Torsion creep curves after pretension at 650°C for 316H stainless steel where experimental data and predicted curves are adapted from [4] and [35], respectively.

where t denotes time and the scalar functions Ψ_1 and Ψ_2 can be determined from creep tests. Note that the temperature effects on the constitutive relations are not incorporated directly and are taken into account when determining the functions Ψ_1 and Ψ_2. The functions Ψ_1 and Ψ_2 were determined also by fitting to the experimental data in [4]. Figure 24 shows a typical comparison for tensile creep test on prestrained specimens. Similar agreement was obtained for torsion creep.

In the phenomenological models described above, creep evolution and prior deformation effect are predicted on the macroscopic scale. These models do not explicitly incorporate creep deformation mechanisms. For example, the authors in [33] considered that creep was governed by the evolution of cavities on grain boundaries and dislocation creep is omitted, while the models [35, 36] can not capture the features of cavity evolution during creep. Although prior deformation effects can be quantified in these models, the observed temperature effects caused by different mechanisms can not be easily accounted for. Therefore, the weaknesses mentioned above limit the application of these phenomenological models in engineering practice. However, recently developed technologies such as crystal plasticity models or multiscale modelling technologies (e.g., [37–42]) have provided a robust framework to numerically quantify the evolution of microstructure of single/multi-phase single crystals and polycrystals during inelastic deformation and to reveal the underlying microstructural mechanisms of deformation and fracture behaviour.

5 Summary

Available experimental data which examine the effect of prior deformation on subsequent high temperature creep have been reviewed. It has been found that prior deformation can introduce both resistance and enhancement effects on the subsequent creep response of metallic materials and may lead to a significant influence on the creep fracture behaviour. The overall effects can be summarised as follows.

1. The introduction of inelastic prestrain can affect the subsequent creep deformation and fracture response.

2. For stainless steel, pretension generally leads to an increase in the subsequent creep resistance, regardless of prestrain temperature, while precompression may lead to an enhancement effect. This load direction effect is also observed in Nimonic 80A for pretorsion.

3. For 2.25Cr-1Mo ferritic steel creep enhancement is seen following prior tensile deformation. This suggests that the effect of prestrain depends on steel composition.

4. The effect of prestrain depend on prestraining temperature for AISI 304 stainless steel, TiAl alloy and the intermetallic Ni_3Al.

5. In most cases examined, a reduction in the Monkman-Grant constant and the creep ductility is observed due to pre-strain. No beneficial effects of prestrain on creep ductility have been reported to date, though under certain conditions some materials show

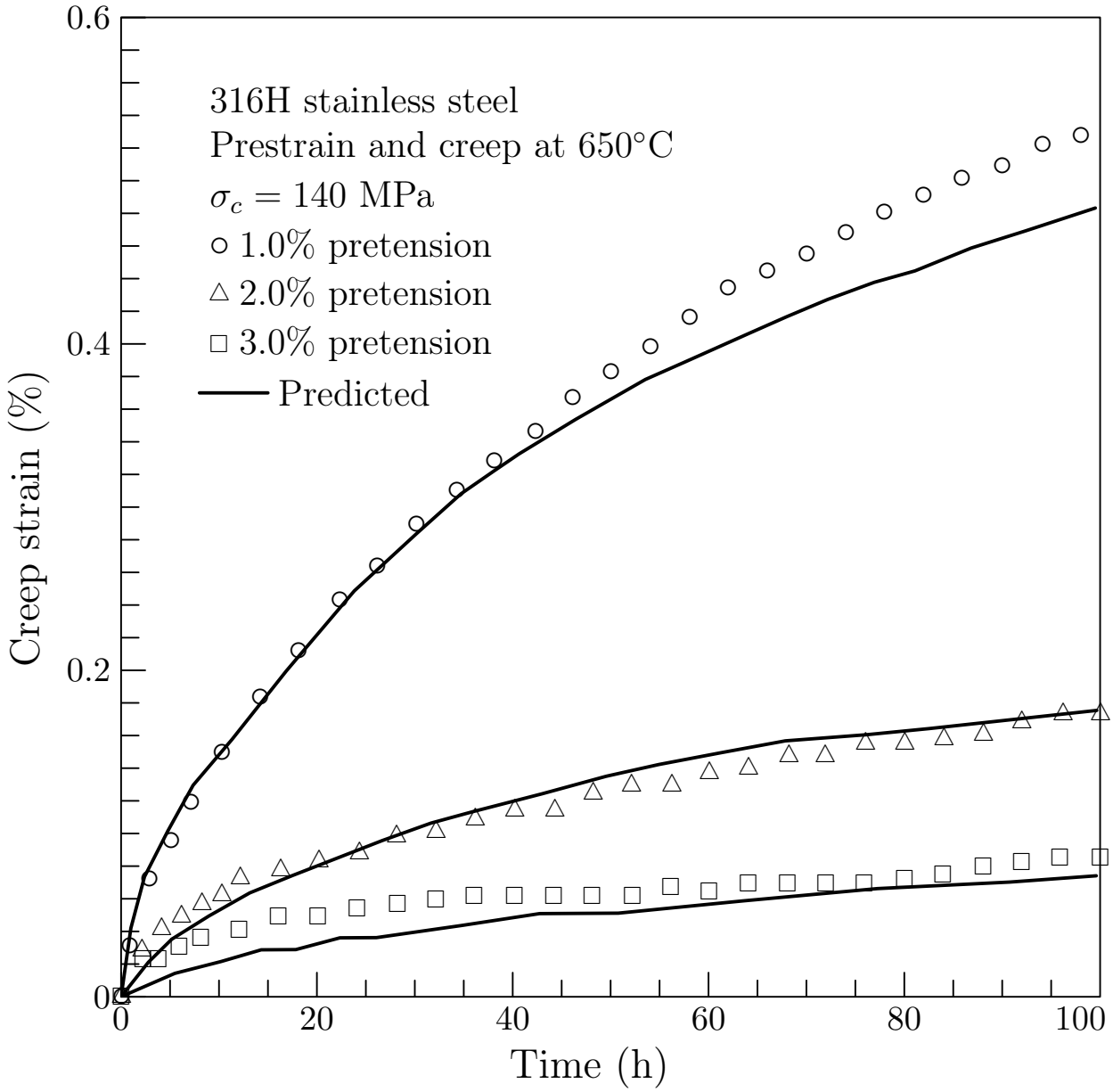

Figure 24: Tensile creep curves after pretension at 650°C for 316H stainless steel where experimental data and predicted curves are adapted from [4] and [36], respectively.

a weak dependence of Monkman-Grant constant (and creep ductility) on prestrain. For 0.5Cr-0.5Mo ferritic steel, pretension can result in an increase of the creep crack growth rate.

6. Explicit interpretations for experimental findings are desirable and require further numerical modelling support. A comprehensive physically based explanation for prestrain effects is lacking, though some insights are provided from consideration of dislocation mechanisms.

Acknowledgments This work was funded by Science Foundation Ireland under grant 08/RFP/ENM1477.

References

[1] Dieter GE. Mechanical Metallurgy, third ed. Mcgraw-Hill Publishing Company; 1986.

[2] Wilshire B, Willis M. Mechanisms of Strain Accumulation and Damage Development during Creep of Prestrained 316 Stainless Steels. Metall Mater Trans A 2004;35A: 563-71.

[3] Zhang YH, Knowles DM. Prestraining effect on creep behavior of nickel base C263 superalloy. Mater Sci Technol 2002;18:917-23.

[4] Ohashi Y, Kawai M, Momose T. Effects of Prior Plasticity on Subsequent Creep of Type 316 Stainless Steel at Elevated Temperature. J Engng Mater Technol-Trans ASME 1986;108:68-74.

[5] Kikuchi S, Ilschner B. Effects of a small prestrain at high temperatures on the creep behaviour of AISI 304 stainless steel. Scripta Metall 1986;20:159-62.

[6] Usami S, Mori T. Creep deformation of austenitic steels at medium and low temperatures. Cryogenics 2000;40:117-26.

[7] Davies PW, Wilshire B, Richards JD. Influence of cold work on creep and fracture behaviour of a dilute nickel alloy. J Inst Met 1962;90(11):431-3.

[8] Marlin RT, Cosandey F, Tien JK. The effect of predeformation on the creep and stress rupture of an oxide dispersion strengthened mechanical alloy. Metall Trans A 1980;11A:1771-5.

[9] Wang JN, Schwartz AJ, Nieh TG, Clemens D. Reduction of primary creep in TiAl alloys by prestraining. Mater Sci Engng A-Struct 1995;206:63-70.

[10] Cairney JM, Rong TS, Jones IP, Smallman RE. Intermediate temperature creep mechanisms in Ni_3Al. Philos Mag 2003;83(15):1827-43.

[11] Davies CM, Dean DW, Nikbin KM. The influence of compressive plastic pre-strain on the creep deformation and damage behaviour of 316H stainless steel. In Proceedings of the International Conference on Engineering Structural Integrity Assessment Its Contribution to the Sustainable Economy, 19th-20th May 2009, Manchester, UK, EMAS Publishing.

[12] Davies CM. Personal communacation. October 6, 2009.

[13] Tai KC, Endo T. Effect of pre-creep on the succeeding creep behavior of a 2.25Cr-1Mo steel. Scripta Metall 1993;29:643-6.

[14] Dyson BF, Loveday MS, Rodgers MJ. Grain boundary cavitation under various states of applied stress. Proc R Soc Lond A 1976;349(1657):245-59.

[15] Loveday MS, Dyson BF. Prestrain-induced particle microcracking and creep cavitation in IN597. Acta Metall 1983;31(3):397-405.

[16] Pandey MC, Mukherjee AK, Taplin MR. Prior deformation effects on creep and fracture in Inconel alloy X-750. Metall Trans A 1984;15A:1437-41.

[17] Rong TS, Jones IP, Smallman RE. Combination tests on TiAl involving constant strain-rate deformation, annealing and creep. Acta Mater 1998;46(13):4507-17.

[18] Li YJ, Zeng XH, Blum W. On the elevated-temperature deformation behavior of polycrystalline Cu subjected to predeformation by multiple compression. Mater Sci Eng A-Struct 2008;483-484:547-50.

[19] Monkman FC, Grant NJ. An empirical relationship between rupture life and minimum creep rate in creep-rupture tests. Proc ASTM 1956;56:593-620.

[20] Willis M, McDonaugh-Smith A, Hales R. Prestrain effects on creep ductility of a 316 stainless steel light forging. Int J Pres Ves Pip 1999;76:355-9.

[21] Auzoux Q, Allais L, Caes C, Girard B, Tournie I, Gourgues AF, Pineau A. Intergranular damage in AISI 316L(N) austenitic stainless steel at 600°C: Pre-strain and multiaxial effects. Nucl Engng Des 2005;235:2227-45.

[22] Shiozawa K, Weertman JR. Studies of nucleation mechanisms and the role of residual stresses in the grain boundary cavitation of a superalloy. Acta Metall 1983;31(7):993-1004.

[23] Worswick D, Pilkington R. The effect of prior damage on creep-crack propagation in Ferritic steels. Proc. 5th Int. Conf. of Strength of Metal; 1979. p. 409-16.

[24] Siverns MJ, Price AT. Crack propagation under creep conditions in a quenched 2 $\frac{1}{4}$ chromium 1 molybdenum steel. Int J Fracture 1973;9:199-207.

[25] Poirier JP. Creep of crystals: High-temperature deformation process in metals, ceramics and minerals, first ed. Cambridge University Press, Cambridge; 1985.

[26] Parker JD, Wilshire B. The effects of prestrain on the creep and fracture behaviour of polycrystalline copper. Mater Sci Engng 1980;43:271-80.

[27] Wilshire B. Creep mechanisms of oxide-dispersion-strengthened alloys. Proc. of 7th Int. Conf. on Creep and Fract. Edited by J. C. Earthman and F. A. Mohamed. The Minerals, Metals & Materials Society; 1997. p. 19-28.

[28] Wilshire B, Palmer CJ. Strain accumlation during creep of prestrained copper. Mater Sci Engng A-Struct 2004;387-389:716-8.

[29] Wilshire B, Burt H, Battenbough AJ. Grain and grain boundary zone contributions to strain accumlation during creep of polycrystalline copper. Mat Sci Engng A-Struct 2005;410-411:16-9.

[30] Goods SH, Brown LM. The nucleation of cavities by plastic deformation. Acta Metall 1979;27:1-15.

[31] Kikuchi M, Shiozawa K, Weertman JR. Void nucleation in astroloy - Theory and experiments. Acta Metall 1981;29:1747-58.

[32] Endo T, Shi JZ. Factors affecting the creep rate and creep life of a 2.25Cr-Mo steel under constant load. Proc 10th Int Conf on Strength of Mater; 1994. p. 665-8.

[33] Murakami S, Sanomura Y, Hattori M, Modelling of the coupled effect of plastic damage and creep damage in Nimonic 80A. Int J Solids Structures 1986;22(4): 373-86.

[34] Hayhurst DR. Creep rupture under multi-axial states of stress. J Mech Phys Solids 1972; 20:381-90.

[35] Xia Z, Ellyin F. A rate-dependent inelastic constitutive model part II: creep deformation including prior plastic strain effects. J Engng Mater Technol-Trans ASME 1991;113:324-8.

[36] Peleshko VA. Applied creep theory for bodies with anisotropy due to plastic prestrain. Mech Solids 2007;42(2):307-320.

[37] Meissonnier FT, Busso EP, O'Dowd NP. Finite element implementation of a generalised non-local rate-dependent crystallographic formulation for finite strains. Int J Plasticity 2001;17:601-40.

[38] Delannay L, Jacques PJ, Kalidindi SR. Finite element modeling of crystal plasticity with grains shaped as truncated octahedrons. Int J Plasticity 2006;22(10):1879-98.

[39] Zhao LG, O'Dowd NP, Busso EP. A coupled kinetic-constitutive approach to the study of high temperature crack initiation in single crystal nicke-base superalloys. J Mech Phys Solids 2006;54:288-309.

[40] Dunne FPE, Rugg D, Walker A. Lengthscale-dependent, elastically anisotropic, physically-based hcp crystal plasticity: Application to cold-dwell fatigue in Ti alloys. Int J Plasticity 2007;23(6):1061-83.

[41] Link T, Epishin A, Fedelich B. Inhomogeneity of misfit stresses in nickel-base superalloys: Effect on propagation of matrix dislocation loops. Philos Mag 2009;89(13):1141-59.

[42] Dyson BF. Microstructure base creep constitutive model for precipitation strengthend alloys: theory and application. Mater Sci Technol 2009; 25(2): 213-20.